Supporting information

An optimal Fe-C coordination ensemble for hydrocarbon chain growth: a full Fischer-Tropsch synthesis mechanism from machine learning

Qian-Yu Liu[1], Dongxiao Chen[1], Cheng Shang[1]*, Zhi-Pan Liu[1,2,3]*

[1]Collaborative Innovation Center of Chemistry for Energy Material, Shanghai Key Laboratory of Molecular Catalysis and Innovative Materials, Key Laboratory of Computational Physical Science, Department of Chemistry, Fudan University, Shanghai 200433, China

[2]Key Laboratory of Synthetic and Self-Assembly Chemistry for Organic Functional Molecules, Shanghai Institute of Organic Chemistry, Chinese Academy of Sciences, Shanghai 200032, China

[3] Shanghai Qi Zhi Institution, Shanghai 200030, China

Contents

1. Theoretical methods

1.1. Construction of Fe–C–H–O quaternary G-NN potential

Architecture of neural network potential

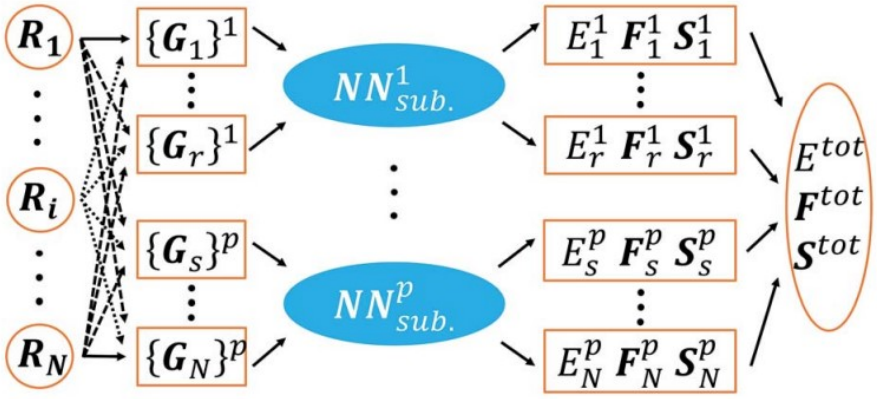

Scheme S1. Scheme for the HDNN architecture. The subscripts *i* and *N* represent atom indices and total number of atoms in a structure. The input of an NN is a set of structural descriptors {$\boldsymbol{G_i}$} constructed from Cartesian coordinates {$\boldsymbol{R}$} of a structure, and the outputs are the atomic properties { E_i, $\boldsymbol{F_i}$, $\boldsymbol{S_i}$ }, i.e. energy, forces and stresses. The overall properties E^{tot}, $\boldsymbol{F^{tot}}$, and $\boldsymbol{S^{tot}}$, can be calculated from the individual atomic contributions.

In this work, we utilized the high dimensional neural network (HDNN) scheme to construct the NN potential[1-4]. The NN architecture is schematically shown in Scheme S1. In Eq. 1, the total energy E^{tot} can be decomposed and written as a linear combination of atomic energy E_i, which is the output of the standard neural network. The input nodes are a set of geometry-based structural descriptors, {$\boldsymbol{G_i}$}.

$$E^{tot} = \sum_i E_i \qquad (1)$$

The atomic force can be analytically derived according to Eq. 2, where the force component $F_{k,a}$, α=x, y or z, acting on the atom *k* is the derivative of the total energy with respect to its coordinate $R_{k,a}$. By combining with Eq. 1, the force component can be further related to the derivatives of the atomic energy with respect to *j*th structural descriptors of atom *i*, $G_{j,i}$:

$$F_{k,\alpha} = -\frac{\partial E^{tot}}{\partial R_{k,\alpha}} = -\sum_{i,j} \frac{\partial E_i}{\partial G_{j,i}} \frac{\partial G_{j,i}}{\partial R_{k,\alpha}} \qquad (2)$$

Similarly, the static stress tensor matrix element $\sigma_{\alpha\beta}$ can be analytically derived as:

$$\sigma_{\alpha\beta} = -\frac{1}{V}\sum_{i,j,d} \frac{(r_d)_\alpha (r_d)_\beta}{r_d} \frac{\partial E_i}{\partial G_{j,i}} \frac{\partial G_{j,i}}{\partial r_d} \qquad (3)$$

where $\mathbf{r_d}$ and r_d are the distance vectors constituting of $G_{j,i}$ and its module, respectively, and *V* is the volume of the structure.

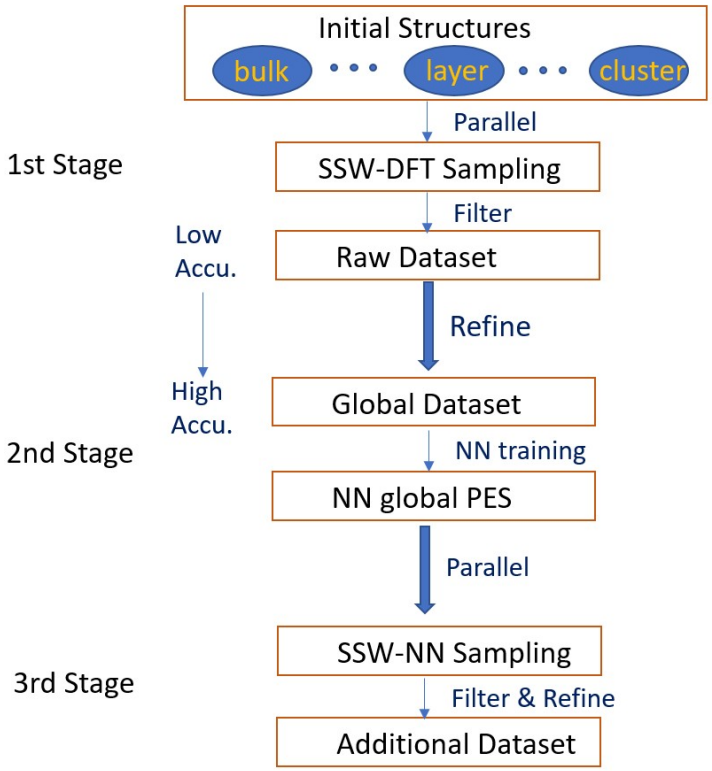

Scheme S2. Procedure for the generation of the global training dataset by SSW global optimization. In the first stage, the SSW sampling is typically performed by low accuracy DFT calculations. In the second stage, the global dataset is first refined with high accuracy DFT setups, and then an NN training is performed based on the accurate global dataset. In the third stage, an additional dataset is generated by SSW sampling utilizing the previously obtained NN PES, and is fed into the global dataset. A new cycle of NN training then starts based on the new global dataset (back to stage 2).

Construction of the global data set using SSW-NN

Undoubtedly, the data set used for training the NN determines largely the quality of the potential energy surface (PES) of G-NN. Our previous works have shown that the stochastic surface walking (SSW) global optimzation[5-7] can be used to fast generate a global data set, which incorporates different structural patterns on the global PES. The SSW PES search is fully automated and does not need a priori knowledge on the system, such as the structure motif (e.g., bonding patterns, symmetry) of materials. The brief description of the Fe−C−H−O global data set in this work is detailed in Table S1, and the G-NN data set and potential can be openly downloaded from http://www.lasphub.com/supportings/Trainfile_FeCHO.tar.gz and http://www.lasphub.com/supportings/FeCHO.pot.

In brief, the SSW-NN method involves three stages for constructing the global data set, as described in the following.

(i) **The first stage** constructs a raw data set, which contains the most common atomic environment and serves as the training data set for building an initial NN PES. This is done by performing density functional theory (DFT) SSW global optimization in a massively parallel way. The DFT calculation is typically with low accuracy setups and restricted to small unit cells to speed up the SSW search. By collecting and screening the structures from the SSW

trajectories, a raw data set is finally obtained. The low accuracy calculations use 300 eV kinetics energy cutoff and 15 $Å^{-1}$ *k*-point auto-mesh (15 $Å^{-1}$ auto-mesh means the first Brillouin zone *k*-point sampling adopted the Monkhorst-Pack scheme with an automated mesh determined by 15 times the reciprocal lattice vectors).

(ii) **The second stage** trains an NN global PES. This is done by first refining the data set using first principles calculation with high accuracy setups, followed by the NN training on the accurate global data set. The high accuracy calculation for producing the data set use 450 eV kinetics energy cutoff and 25 $Å^{-1}$ *k*-point auto-mesh. The NN architecture applied in this stage utilizes a small set of structural descriptors and a small network size.

(iii) **The third stage** iteratively expands the global data set. It targets to increase the predictive power of NN PES by incorporating more structural patterns into the data set. This is done by carrying out SSW PES search using the NN potential obtained in the second stage, starting from a variety of initial structures. These initial structures are often randomly configurated and also include large systems with many atoms per unit cell. The structures from all SSW trajectories are collected and filtered to generate the additional data set. This new data set is then fed to the global data set (back to stage 2) to start a new cycle of NN training.

Table S1. Structure information of the global PES data set for G-NN potential training. The listed data is the number of structures in the data set, as distinguished by the chemical formula, the number of atoms per cell (N_{atom}) and the type of structure, including cluster ($N_{cluster}$), layer (N_{layer}) and bulk (N_{bulk}). The total numbers of the structure (N_{total}) are also summarized.

Species	N_{atom}	$N_{cluster}$	N_{layer}	N_{bulk}	N_{total}
Fe4	4	0	0	10	10
Fe16	16	70	81	476	627
Fe28	28	0	0	12	12
Fe29	29	0	0	33	33
Fe30	30	0	0	85	85
Fe31	31	0	0	168	168
Fe32	32	0	27	204	231
Fe60	60	0	1	16	17
Fe61	61	0	0	11	11
Fe62	62	0	0	14	14
Fe127	127	0	0	280	280
Fe128	128	0	0	1	1
O1-Fe3	4	0	0	1	1
O1-Fe15	16	1	2	10	13
O2-Fe11	13	0	1	0	1
O2-Fe14	16	0	4	10	14
O2-Fe30	32	0	2	0	2
O4	4	0	37	0	37
O11	11	0	195	96	291
C1-Fe12	13	0	39	0	39
C1-Fe18	19	0	81	240	321
C1-Fe31	32	0	122	1	123

C1-O1-Fe11	13	0	2	0	2
C1-O1-Fe17	19	0	4	8	12
C1-O1-Fe30	32	0	2	0	2
C1-O2-Fe9	12	0	1	0	1
C1-O2-Fe16	19	0	2	6	8
C1-O2-Fe29	32	0	1	0	1
C2-Fe10	12	0	53	0	53
C2-Fe17	19	0	0	30	30
C2-Fe25	27	0	0	1	1
C2-Fe29	31	0	0	10	10
C2-Fe36	38	0	21	0	21
C2-O1-Fe9	12	0	3	0	3
C2-O1-Fe16	19	0	0	1	1
C2-O2-Fe8	12	0	1	0	1
C2-O2-Fe15	19	0	0	1	1
C2-O2-Fe34	38	0	1	0	1
C3-Fe16	19	5	0	0	5
C3-O1-Fe8	12	0	0	1	1
C3-O2-Fe7	12	0	0	2	2
C4-Fe8	12	0	0	182	182
C4-Fe12	16	0	0	41	41
C4-Fe25	29	0	0	1	1
C4-O1-Fe7	12	0	0	3	3
C4-O2-Fe6	12	0	0	2	2
C5-Fe14	19	0	10	4	14
C5-O1-Fe12	18	0	0	2	2
C5-O1-Fe13	19	0	1	0	1
C5-O1-Fe14	20	0	0	3	3
C5-O1-Fe23	29	0	1	0	1
C5-O2-Fe11	18	0	2	1	3
C5-O2-Fe13	20	0	2	0	2
C5-O2-Fe14	21	0	1	1	2
C5-O2-Fe22	29	0	0	3	3
C5-O2-Fe24	31	0	1	0	1
C6-Fe10	16	0	1	8	9
C6-Fe12	18	0	117	104	221
C6-Fe14	20	0	109	119	228
C6-Fe15	21	0	77	123	200
C6-Fe23	29	0	89	197	286
C6-Fe24	30	0	0	104	104
C6-Fe25	31	0	120	260	380
C6-O1-Fe9	16	0	0	2	2
C6-O1-Fe11	18	0	2	4	6
C6-O1-Fe13	20	0	2	1	3
C6-O1-Fe14	21	0	3	2	5

C6-O1-Fe22	29	0	1	2	3
C6-O1-Fe24	31	0	1	2	3
C6-O2-Fe10	18	0	3	3	6
C6-O2-Fe12	20	0	4	2	6
C6-O2-Fe13	21	0	1	3	4
C6-O2-Fe21	29	0	1	8	9
C6-O2-Fe23	31	0	2	3	5
C7-Fe16	23	0	0	24	24
C7-O2-Fe11	20	0	0	1	1
C7-O2-Fe15	24	1	0	0	1
C8	8	0	17	289	306
C8-Fe12	20	0	8	36	44
C8-Fe16	24	3	0	33	36
C8-Fe20	28	0	0	52	52
C9-Fe15	24	0	15	30	45
C9-O1-Fe14	24	0	1	0	1
C9-O2-Fe9	20	0	0	1	1
C9-O2-Fe12	23	0	0	1	1
C10-Fe10	20	0	21	40	61
C10-Fe13	23	0	0	17	17
C10-Fe22	32	0	0	84	84
C10-Fe27	37	0	9	0	9
C10-Fe28	38	0	3	1	4
C10-Fe30	40	0	8	8	16
C10-O1-Fe9	20	0	1	0	1
C10-O2-Fe8	20	0	1	1	2
C10-O2-Fe16	28	0	0	1	1
C11-Fe28	39	0	10	3	13
C11-O1-Fe27	39	0	1	0	1
C11-O1-Fe30	42	0	161	17	178
C11-O2-Fe27	40	0	1	0	1
C11-O2-Fe29	42	0	1	0	1
C12-Fe16	28	0	20	61	81
C12-Fe20	32	0	0	64	64
C12-Fe24	36	0	25	0	25
C12-Fe26	38	0	8	1	9
C12-Fe27	39	0	3	1	4
C12-Fe28	40	0	75	321	396
C12-Fe30	42	0	27	0	27
C12-Fe46	58	0	23	0	23
C12-Fe50	62	0	19	0	19
C12-O1-Fe27	40	0	0	1	1
C12-O2-Fe14	28	0	1	1	2
C12-O2-Fe26	40	0	1	1	2
C12-O2-Fe28	42	0	136	0	136

C13-O1-Fe28	42	0	51	0	51
C13-O1-Fe30	44	0	44	1	45
C14-O1-Fe29	44	0	49	0	49
C15-O2-Fe25	42	0	2	0	2
C16-Fe24	40	0	0	106	106
C16-Fe26	42	0	111	0	111
C16-O2-Fe24	42	0	1	0	1
C17-Fe41	58	0	97	1	98
C18-O2-Fe16	36	0	2	0	2
C19-Fe17	36	0	122	1	123
C19-O1-Fe16	36	0	1	0	1
C19-O2-Fe15	36	0	2	0	2
C22-Fe55	77	0	1	1	2
C22-Fe56	78	0	3	0	3
C24-Fe51	75	0	3	1	4
C24-Fe52	76	0	4	1	5
C24-Fe53	77	0	3	1	4
C24-Fe54	78	0	3	2	5
C25-Fe11	36	0	49	1	50
C28-Fe16	44	0	33	3	36
C30-O2-Fe72	104	0	23	0	23
C30-O2-Fe74	106	0	61	0	61
C32-Fe64	96	0	1	0	1
C32-Fe74	106	0	18	0	18
C32-O1-Fe64	97	0	1	0	1
C32-O2-Fe74	108	0	90	0	90
C33-O1-Fe74	108	0	98	0	98
C34-O1-Fe74	109	0	72	0	72
C35-Fe80	115	0	3	0	3
C36-Fe80	116	0	1	0	1
C36-O1-Fe80	117	0	137	0	137
C37-O1-Fe80	118	0	253	0	253
C38-Fe16	54	0	23	0	23
C39-Fe120	159	0	3	0	3
C40-Fe16	56	0	23	0	23
C40-O1-Fe96	137	0	24	0	24
C41-Fe120	161	0	12	0	12
C41-O5-Fe80	126	0	1	0	1
C42-Fe120	162	0	20	0	20
C42-O6-Fe80	128	0	1	0	1
C43-Fe96	139	0	8	0	8
C43-O7-Fe80	130	0	19	0	19
C44-Fe16	60	0	50	1	51
C44-Fe96	140	0	4	0	4
C44-O1-Fe80	125	0	10	0	10

C44-O1-Fe96	141	0	11	0	11
C47-Fe84	131	0	1	0	1
C47-Fe96	143	0	85	0	85
C47-Fe112	159	0	20	0	20
C47-Fe120	167	0	11	0	11
C48-Fe84	132	0	1	0	1
C48-O1-Fe84	133	0	85	0	85
C49-Fe96	145	0	21	0	21
C49-Fe112	161	0	27	0	27
C49-Fe120	169	0	5	0	5
C49-O1-Fe84	134	0	24	0	24
C49-O1-Fe120	170	0	170	0	170
C49-O2-Fe112	163	0	1	0	1
C50-Fe96	146	0	16	0	16
C50-Fe112	162	0	16	0	16
C50-Fe120	170	0	8	0	8
C52-O4-Fe112	168	0	8	0	8
C53-O5-Fe112	170	0	53	0	53
C60-O4-Fe144	208	0	3	0	3
C60-O4-Fe148	212	0	3	0	3
C64-Fe148	212	0	1	0	1
C64-O1-Fe136	201	0	8	0	8
C64-O4-Fe148	216	0	4	0	4
C104-O1-Fe224	329	0	10	0	10
H1-Fe15	16	0	0	23	23
H1-Fe16	17	0	0	1	1
H1-Fe23	24	0	5	0	5
H1-Fe26	27	0	10	0	10
H1-Fe27	28	0	6	0	6
H1-Fe31	32	0	0	3	3
H1-O2-Fe13	16	0	0	1	1
H1-C1-Fe30	32	0	52	1	53
H1-C5-Fe18	24	0	0	7	7
H1-C6-O2-Fe15	24	0	1	0	1
H1-C7-O1-Fe15	24	0	2	0	2
H1-C7-O2-Fe10	20	0	3	0	3
H1-C8-Fe11	20	0	67	2	69
H1-C8-Fe15	24	0	96	2	98
H1-C8-O1-Fe10	20	0	4	0	4
H1-C8-O1-Fe14	24	0	1	0	1
H1-C8-O2-Fe9	20	0	7	0	7
H1-C9-Fe10	20	0	440	56	496
H1-C9-O1-Fe9	20	0	4	0	4
H1-C9-O2-Fe8	20	0	7	0	7
H1-C9-O2-Fe16	28	0	2	0	2

H1-C10-O1-Fe16	28	0	3	0	3
H1-C10-O2-Fe15	28	0	6	0	6
H1-C11-Fe16	28	0	234	44	278
H1-C11-O1-Fe15	28	0	1	1	2
H1-C11-O2-Fe14	28	0	3	2	5
H1-C11-O2-Fe28	42	0	270	2	272
H1-C12-O1-Fe28	42	0	95	0	95
H1-C32-O1-Fe64	98	0	10	0	10
H1-C37-O1-Fe80	119	0	17	0	17
H1-C40-O4-Fe80	125	0	4	0	4
H1-C41-Fe120	162	0	1	0	1
H1-C41-O1-Fe96	139	0	4	0	4
H1-C42-Fe120	163	0	13	0	13
H1-C45-O1-Fe96	143	0	18	0	18
H1-C48-Fe84	133	0	2	0	2
H1-C48-O1-Fe84	134	0	26	0	26
H1-C49-Fe96	146	0	17	0	17
H1-C49-Fe112	162	0	21	0	21
H1-C49-Fe120	170	0	1	0	1
H1-C49-O1-Fe120	171	0	198	0	198
H1-C50-Fe96	147	0	3	0	3
H1-C50-Fe112	163	0	5	0	5
H1-C50-Fe120	171	0	9	0	9
H2	2	1	0	0	1
H2-Fe14	16	0	5	42	47
H2-Fe16	18	0	88	91	179
H2-Fe21	23	0	0	10	10
H2-Fe22	24	0	1	0	1
H2-Fe27	29	1	1	5	7
H2-Fe28	30	0	5	0	5
H2-Fe30	32	1	0	2	3
H2-O1-Fe13	16	0	0	2	2
H2-O1-Fe15	18	0	6	3	9
H2-O2-Fe14	18	0	0	4	4
H2-C1	3	4	0	0	4
H2-C1-O1	4	103	0	0	103
H2-C1-O2	5	40	0	0	40
H2-C1-O2-Fe12	17	0	15	1	16
H2-C1-O2-Fe16	21	0	10	0	10
H2-C1-O2-Fe20	25	0	4	0	4
H2-C1-O2-Fe36	41	0	11	0	11
H2-C1-O3	6	11	0	0	11
H2-C1-O3-Fe36	42	0	3	0	3
H2-C2	4	86	0	0	86
H2-C2-Fe18	22	0	0	16	16

H2-C2-O2-Fe16	22	0	0	2	2
H2-C2-O3-Fe26	33	0	1	0	1
H2-C2-O3-Fe27	34	0	7	0	7
H2-C3-Fe17	22	0	0	17	17
H2-C3-O1-Fe23	29	0	1	0	1
H2-C3-O2-Fe22	29	0	0	4	4
H2-C3-O2-Fe26	33	0	9	0	9
H2-C3-O2-Fe27	34	0	5	0	5
H2-C4-Fe18	24	0	0	16	16
H2-C4-Fe23	29	0	99	214	313
H2-C4-O1-Fe22	29	0	0	4	4
H2-C4-O1-Fe26	33	0	1	0	1
H2-C4-O1-Fe27	34	0	5	0	5
H2-C4-O2-Fe21	29	0	0	5	5
H2-C4-O3	9	60	0	0	60
H2-C4-O4	10	2	0	0	2
H2-C4-O5	11	8	0	0	8
H2-C5-Fe18	25	0	0	10	10
H2-C5-O2-Fe13	22	0	0	1	1
H2-C5-O2-Fe15	24	0	0	1	1
H2-C5-O3	10	6	0	0	6
H2-C5-O4	11	4	0	0	4
H2-C6-Fe16	24	0	0	15	15
H2-C6-O1-Fe13	22	0	2	5	7
H2-C6-O2	10	2	0	0	2
H2-C6-O2-Fe12	22	0	2	0	2
H2-C6-O2-Fe17	27	0	0	1	1
H2-C7-Fe10	19	0	21	5	26
H2-C7-Fe13	22	0	99	258	357
H2-C7-Fe18	27	0	0	28	28
H2-C7-O1	10	2	0	0	2
H2-C7-O1-Fe10	20	0	2	0	2
H2-C7-O1-Fe12	22	0	0	6	6
H2-C7-O2-Fe9	20	0	3	0	3
H2-C7-O2-Fe11	22	0	1	4	5
H2-C7-O2-Fe16	27	0	0	2	2
H2-C8-Fe10	20	0	68	6	74
H2-C8-O1-Fe9	20	0	1	1	2
H2-C8-O2-Fe8	20	0	2	0	2
H2-C9-Fe13	24	0	0	12	12
H2-C9-Fe16	27	0	0	10	10
H2-C9-O2-Fe15	28	0	1	0	1
H2-C10-Fe16	28	0	16	3	19
H2-C10-O1-Fe15	28	0	0	1	1
H2-C11-O1-Fe28	42	0	163	0	163

H2-C12-Fe28	42	0	55	0	55
H2-C12-Fe48	62	0	42	0	42
H2-C13-Fe30	45	0	49	0	49
H2-C13-O1-Fe28	44	0	268	0	268
H2-C14-Fe28	44	0	39	0	39
H2-C14-Fe33	49	0	43	0	43
H2-C20-Fe40	62	0	28	0	28
H2-C25-Fe35	62	0	89	0	89
H2-C30-Fe74	106	0	14	0	14
H2-C32-Fe64	98	0	36	0	36
H2-C32-Fe74	108	0	60	0	60
H2-C32-O1-Fe74	109	0	47	0	47
H2-C33-O1-Fe64	100	0	2	0	2
H2-C36-Fe80	118	0	276	0	276
H2-C40-O4-Fe80	126	0	1	0	1
H2-C40-O5-Fe80	127	0	72	0	72
H2-C41-O4-Fe80	127	0	4	0	4
H2-C41-O6-Fe80	129	0	32	0	32
H2-C42-Fe120	164	0	5	0	5
H2-C49-Fe96	147	0	21	0	21
H2-C49-Fe112	163	0	11	0	11
H2-C49-Fe120	171	0	12	0	12
H2-C50-Fe112	164	0	17	0	17
H2-C50-Fe120	172	0	13	0	13
H3-Fe26	29	0	4	0	4
H3-Fe29	32	0	0	1	1
H3-O2-Fe24	29	0	1	0	1
H3-C1	4	7	0	0	7
H3-C1-O1-Fe15	20	0	20	1	21
H3-C1-O1-Fe16	21	0	16	0	16
H3-C1-O1-Fe20	25	0	4	0	4
H3-C1-O2-Fe15	21	0	13	0	13
H3-C1-O2-Fe16	22	0	18	0	18
H3-C1-O2-Fe36	42	0	3	0	3
H3-C1-O3-Fe35	42	0	1	0	1
H3-C2-Fe22	27	0	0	13	13
H3-C2-Fe33	38	0	45	2	47
H3-C2-O2-Fe26	33	0	2	0	2
H3-C2-O2-Fe27	34	0	4	0	4
H3-C2-O3-Fe34	42	0	10	0	10
H3-C2-O3-Fe36	44	0	15	0	15
H3-C2-O4-Fe32	41	0	1	0	1
H3-C2-O4-Fe33	42	0	3	0	3
H3-C2-O4-Fe35	44	0	4	0	4
H3-C3-O1-Fe27	34	0	5	0	5

H3-C3-O2-Fe25	33	0	2	0	2
H3-C3-O3-Fe35	44	0	5	1	6
H3-C4-O2-Fe16	25	0	0	1	1
H3-C5-O1-Fe16	25	0	0	1	1
H3-C5-O2-Fe15	25	0	0	2	2
H3-C6-Fe16	25	0	102	226	328
H3-C6-Fe22	31	0	0	4	4
H3-C6-O1-Fe15	25	0	3	3	6
H3-C6-O2-Fe14	25	0	0	5	5
H3-C8-Fe14	25	0	0	6	6
H3-C12-O2-Fe36	53	0	156	0	156
H3-C13-Fe40	56	0	41	0	41
H3-C13-O2-Fe35	53	0	276	0	276
H3-C13-O2-Fe36	54	0	219	0	219
H3-C14-O2-Fe35	54	0	183	0	183
H3-C14-O2-Fe36	55	0	498	0	498
H3-C15-O1-Fe35	54	0	283	0	283
H3-C15-O1-Fe36	55	0	280	0	280
H3-C15-O2-Fe35	55	0	166	0	166
H3-C16-Fe35	54	0	133	0	133
H3-C16-Fe36	55	0	141	0	141
H3-C32-O1-Fe74	110	0	197	0	197
H3-C33-O1-Fe64	101	0	79	0	79
H3-C40-O6-Fe80	129	0	21	0	21
H3-C41-Fe120	164	0	6	0	6
H3-C41-O4-Fe80	128	0	35	0	35
H3-C49-Fe96	148	0	33	0	33
H3-C49-Fe112	164	0	5	0	5
H3-C49-Fe120	172	0	7	0	7
H3-C49-O1-Fe112	165	0	13	0	13
H3-C50-Fe120	173	0	20	0	20
H3-C50-O2-Fe112	167	0	13	0	13
H4-Fe12	16	232	0	13	245
H4-Fe17	21	0	0	12	12
H4-Fe20	24	0	4	0	4
H4-Fe24	28	0	2	0	2
H4-Fe32	36	0	26	0	26
H4-O1-Fe11	16	10	0	0	10
H4-O2-Fe10	16	8	0	0	8
H4-O2-Fe15	21	0	0	1	1
H4-O2-Fe18	24	0	1	0	1
H4-O2-Fe30	36	0	1	0	1
H4-C1	5	128	0	0	128
H4-C1-Fe31	36	0	98	2	100
H4-C1-Fe36	41	0	36	0	36

H4-C1-O1	6	36	0	0	36
H4-C1-O1-Fe16	22	0	29	0	29
H4-C1-O1-Fe30	36	0	2	0	2
H4-C1-O1-Fe35	41	0	1	0	1
H4-C1-O2	7	0	7	0	7
H4-C1-O2-Fe29	36	0	2	0	2
H4-C1-O2-Fe36	43	0	1	0	1
H4-C1-O3-Fe36	44	0	3	0	3
H4-C2	6	34	0	0	34
H4-C2-O1	7	157	0	0	157
H4-C2-O1-Fe15	22	0	8	0	8
H4-C2-O2	8	51	3	4	58
H4-C2-O2-Fe33	41	0	21	2	23
H4-C2-O3-Fe32	41	0	3	0	3
H4-C2-O3-Fe34	43	0	1	0	1
H4-C2-O4-Fe36	46	0	8	0	8
H4-C3	7	52	0	0	52
H4-C3-O1	8	12	0	0	12
H4-C3-O2	9	1	0	0	1
H4-C4	8	119	0	0	119
H4-C4-Fe16	24	0	0	15	15
H4-C4-O2	10	6	0	0	6
H4-C4-O3	11	2	0	0	2
H4-C4-O4	12	4	0	0	4
H4-C4-O4-Fe36	48	0	0	2	2
H4-C4-O5	13	1	0	0	1
H4-C5-O1-Fe14	24	0	0	1	1
H4-C5-O2	11	3	0	0	3
H4-C5-O3	12	21	0	0	21
H4-C5-O4	13	26	0	0	26
H4-C6-Fe14	24	0	0	13	13
H4-C6-O1	11	7	0	0	7
H4-C6-O2	12	22	0	0	22
H4-C6-O3	13	46	0	0	46
H4-C7	11	3	0	0	3
H4-C7-O1	12	6	0	0	6
H4-C7-O2	13	54	0	0	54
H4-C8-Fe46	58	0	15	1	16
H4-C8-O1	13	24	0	0	24
H4-C8-O2-Fe30	44	0	47	0	47
H4-C9	13	1	0	0	1
H4-C9-O2-Fe26	41	0	53	0	53
H4-C9-O2-Fe27	42	0	35	0	35
H4-C10-O2-Fe30	46	0	19	0	19
H4-C11-O2-Fe23	40	0	1	0	1

H4-C11-O2-Fe27	44	0	45	0	45
H4-C11-O2-Fe29	46	0	38	0	38
H4-C12-Fe24	40	0	130	0	130
H4-C12-Fe28	44	0	50	0	50
H4-C12-Fe30	46	0	13	0	13
H4-C12-Fe34	50	0	40	0	40
H4-C12-Fe36	52	0	36	2	38
H4-C12-Fe40	56	0	48	2	50
H4-C12-Fe42	58	0	39	0	39
H4-C12-O1-Fe23	40	0	1	0	1
H4-C12-O1-Fe27	44	0	1	0	1
H4-C12-O2-Fe19	37	0	1	0	1
H4-C12-O2-Fe26	44	0	1	0	1
H4-C12-O2-Fe28	46	0	46	0	46
H4-C12-O2-Fe29	47	0	37	0	37
H4-C13-Fe20	37	0	26	0	26
H4-C13-O2-Fe19	38	0	1	0	1
H4-C13-O2-Fe25	44	0	1	0	1
H4-C14-Fe20	38	0	19	0	19
H4-C14-Fe26	44	0	53	2	55
H4-C14-Fe40	58	0	69	0	69
H4-C14-O1-Fe35	54	0	69	0	69
H4-C15-O2-Fe19	40	0	1	0	1
H4-C16-Fe19	39	0	22	0	22
H4-C16-Fe20	40	0	34	2	36
H4-C17-Fe19	40	0	42	0	42
H4-C17-Fe23	44	0	161	1	162
H4-C17-O1-Fe22	44	0	1	0	1
H4-C17-O2-Fe21	44	0	1	0	1
H4-C20-Fe31	55	0	12	4	16
H4-C20-Fe32	56	0	6	0	6
H4-C32-O1-Fe74	111	0	109	0	109
H4-C33-O1-Fe64	102	0	18	0	18
H4-C39-O1-Fe80	124	0	3	0	3
H4-C40-Fe16	60	0	63	0	63
H4-C41-O4-Fe80	129	0	28	0	28
H4-C49-O1-Fe112	166	0	23	0	23
H4-C50-Fe120	174	0	1	0	1
H4-C50-O1-Fe112	167	0	7	0	7
H4-C64-Fe148	216	0	4	0	4
H4-C64-O2-Fe148	218	0	1	0	1
H5-Fe16	21	0	10	0	10
H5-Fe27	32	0	2	0	2
H5-O2-Fe14	21	0	1	0	1
H5-C1-O2-Fe35	43	0	16	4	20

H5-C1-O3-Fe36	45	0	2	0	2
H5-C2-Fe21	28	0	0	11	11
H5-C2-Fe36	43	0	18	0	18
H5-C2-O2-Fe34	43	0	1	0	1
H5-C3-O2-Fe18	28	0	0	1	1
H5-C4-Fe19	28	0	0	33	33
H5-C6-Fe20	31	0	0	6	6
H5-C10-O1-Fe29	45	0	39	0	39
H5-C11-O1-Fe29	46	0	34	0	34
H5-C13-Fe35	53	0	151	0	151
H5-C14-Fe36	55	0	161	0	161
H5-C15-Fe20	40	0	24	0	24
H5-C15-Fe35	55	0	92	0	92
H5-C15-O1-Fe36	57	0	326	0	326
H5-C15-O2-Fe18	40	0	1	0	1
H5-C16-Fe36	57	0	119	0	119
H5-C32-Fe74	111	0	90	0	90
H5-C39-O1-Fe80	125	0	15	0	15
H5-C41-O4-Fe80	130	0	46	0	46
H5-C49-O1-Fe112	167	0	6	0	6
H5-C50-Fe120	175	0	6	0	6
H5-C50-O1-Fe112	168	0	24	0	24
H6-Fe10	16	0	0	24	24
H6-Fe15	21	0	9	0	9
H6-Fe16	22	0	87	82	169
H6-Fe25	31	0	54	130	184
H6-Fe26	32	15	8	11	34
H6-O1-Fe9	16	0	0	1	1
H6-O1-Fe14	21	0	1	0	1
H6-O1-Fe15	22	0	3	1	4
H6-O1-Fe24	31	0	3	4	7
H6-O1-Fe25	32	1	0	0	1
H6-O2-Fe14	22	0	2	3	5
H6-O2-Fe23	31	0	1	4	5
H6-O2-Fe24	32	0	0	1	1
H6-C1-O1-Fe33	41	0	7	0	7
H6-C1-O1-Fe35	43	0	7	0	7
H6-C1-O2-Fe36	45	0	1	0	1
H6-C1-O3-Fe36	46	0	4	0	4
H6-C2	8	292	0	0	292
H6-C2-Fe36	44	0	27	0	27
H6-C2-O1	9	23	16	20	59
H6-C2-O2-Fe30	40	0	0	1	1
H6-C2-O2-Fe31	41	0	6	3	9
H6-C2-O2-Fe32	42	0	44	10	54

H6-C2-O2-Fe34	44	0	1	0	1
H6-C3	9	88	0	0	88
H6-C3-O1	10	2	0	0	2
H6-C3-O2	11	60	0	0	60
H6-C4	10	29	0	0	29
H6-C4-O2	12	1	0	0	1
H6-C4-O3	13	5	0	0	5
H6-C4-O4	14	3	0	0	3
H6-C5-O2	13	18	0	0	18
H6-C5-O3	14	40	0	0	40
H6-C5-O4	15	51	0	0	51
H6-C6	12	78	0	0	78
H6-C6-O1	13	422	0	0	422
H6-C6-O2	14	75	0	0	75
H6-C6-O3	15	29	0	0	29
H6-C7-O1	14	8	0	0	8
H6-C7-O2	15	19	0	0	19
H6-C7-O4	17	0	3	0	3
H6-C8	14	3	0	0	3
H6-C8-Fe48	62	0	22	0	22
H6-C8-O1	15	7	0	0	7
H6-C9	15	2	0	0	2
H6-C12-Fe32	50	0	34	0	34
H6-C12-O1-Fe23	42	0	1	0	1
H6-C12-O1-Fe31	50	0	1	0	1
H6-C12-O2-Fe30	50	0	1	0	1
H6-C13-Fe23	42	0	66	0	66
H6-C13-O1-Fe22	42	0	1	0	1
H6-C13-O2-Fe21	42	0	2	0	2
H6-C14-O1-Fe35	56	0	149	0	149
H6-C16-O1-Fe27	50	0	2	0	2
H6-C17-Fe27	50	0	123	0	123
H6-C17-O2-Fe25	50	0	1	0	1
H6-C21-Fe35	62	0	62	0	62
H6-C26-O4-Fe72	108	0	3	0	3
H6-C28-O4-Fe72	110	0	2	0	2
H6-C32-Fe72	110	0	1	0	1
H6-C37-O1-Fe80	124	0	3	0	3
H6-C41-O4-Fe80	131	0	4	0	4
H7-Fe16	23	0	0	1	1
H7-Fe25	32	0	0	6	6
H7-O2-Fe23	32	0	0	1	1
H7-C1-O4-Fe34	46	0	1	1	2
H7-C2-Fe29	38	0	32	0	32
H7-C2-Fe35	44	0	11	0	11

H7-C2-Fe36	45	0	36	0	36
H7-C2-O2-Fe27	38	0	1	0	1
H7-C2-O2-Fe31	42	0	14	6	20
H7-C2-O2-Fe32	43	0	12	3	15
H7-C2-O2-Fe34	45	0	1	0	1
H7-C2-O2-Fe36	47	0	7	0	7
H7-C2-O5-Fe34	48	0	0	5	5
H7-C10-Fe36	53	0	77	0	77
H7-C14-Fe30	51	0	44	1	45
H7-C14-Fe35	56	0	314	0	314
H7-C15-Fe35	57	0	247	0	247
H7-C16-Fe34	57	0	39	0	39
H7-C23-Fe47	77	0	14	1	15
H7-C37-O1-Fe80	125	0	1	0	1
H8-Fe8	16	208	0	113	321
H8-Fe16	24	0	1	0	1
H8-Fe20	28	0	2	0	2
H8-O1-Fe7	16	9	0	5	14
H8-O2-Fe6	16	4	0	3	7
H8-C1-Fe27	36	0	70	1	71
H8-C1-O5-Fe36	50	0	1	1	2
H8-C2	10	0	1	0	1
H8-C2-O2	12	0	7	0	7
H8-C2-O2-Fe32	44	0	3	1	4
H8-C2-O2-Fe36	48	0	4	0	4
H8-C2-O3	13	0	6	0	6
H8-C2-O4-Fe34	48	0	5	1	6
H8-C2-O4-Fe35	49	0	2	0	2
H8-C2-O4-Fe36	50	0	7	0	7
H8-C3	11	4	0	0	4
H8-C3-O1-Fe36	48	0	6	0	6
H8-C3-O3	14	2	0	0	2
H8-C4-O1	13	4	0	0	4
H8-C5-O1	14	166	0	0	166
H8-C5-O3	16	10	0	0	10
H8-C5-O4	17	13	0	0	13
H8-C6-O1	15	8	0	0	8
H8-C6-O2	16	10	0	0	10
H8-C6-O3	17	27	0	0	27
H8-C7	15	3	0	0	3
H8-C7-Fe21	36	0	10	0	10
H8-C7-O1	16	11	0	0	11
H8-C7-O2	17	56	0	0	56
H8-C7-O3	18	0	3	4	7
H8-C8	16	6	0	0	6

H8-C8-Fe42	58	0	25	0	25
H8-C8-O1	17	53	0	0	53
H8-C8-O2	18	2	0	0	2
H8-C8-O3	19	0	6	2	8
H8-C9	17	19	0	0	19
H8-C9-O3	20	73	0	0	73
H8-C12-O1-Fe23	44	0	1	0	1
H8-C12-O6	26	0	2	0	2
H8-C13-Fe23	44	0	85	1	86
H8-C13-O1-Fe22	44	0	1	0	1
H8-C16-Fe38	62	0	37	0	37
H8-C19-Fe35	62	0	96	0	96
H8-C28-O2-Fe70	108	0	2	0	2
H8-C37-Fe80	125	0	5	0	5
H8-C37-O1-Fe80	126	0	19	0	19
H8-C38-O1-Fe80	127	0	9	0	9
H9-Fe23	32	12	0	0	12
H9-C2-Fe16	27	0	2	0	2
H9-C2-O1-Fe34	46	0	1	0	1
H9-C2-O1-Fe35	47	0	0	2	2
H9-C2-O1-Fe36	48	0	7	0	7
H9-C3-O1-Fe35	48	0	3	0	3
H9-C9-O1	19	210	0	0	210
H9-C12-Fe30	51	0	38	0	38
H9-C13-Fe17	39	0	28	1	29
H9-C16-O2-Fe23	50	0	2	0	2
H9-C17-Fe24	50	0	55	2	57
H9-C17-O1-Fe23	50	0	0	1	1
H9-C17-O2-Fe22	50	0	1	0	1
H9-C22-Fe46	77	0	7	2	9
H9-C30-Fe70	109	0	2	0	2
H9-C37-O1-Fe80	127	0	28	0	28
H9-C38-O1-Fe80	128	0	21	0	21
H10-Fe21	31	0	8	13	21
H10-Fe22	32	0	11	17	28
H10-O1-Fe20	31	0	0	1	1
H10-O1-Fe21	32	0	1	1	2
H10-C4-O3	17	0	7	0	7
H10-C5-O4	19	3	0	0	3
H10-C5-O5	20	3	0	0	3
H10-C6	16	26	0	0	26
H10-C6-O1	17	3	0	0	3
H10-C6-O2	18	7	0	0	7
H10-C6-O3	19	10	0	0	10
H10-C7	17	3	0	0	3

H10-C7-O1	18	52	0	0	52
H10-C7-O2	19	34	0	0	34
H10-C7-O3	20	0	1	0	1
H10-C8	18	12	0	0	12
H10-C8-O1	19	36	0	0	36
H10-C8-O2	20	0	12	1	13
H10-C8-O3	21	0	1	1	2
H10-C9	19	65	0	0	65
H10-C9-O2	21	0	5	3	8
H10-C10-O1	21	0	3	1	4
H10-C12-O6	28	0	2	1	3
H10-C13-O5	28	0	6	7	13
H10-C26-Fe70	106	0	1	0	1
H10-C28-Fe72	110	0	1	0	1
H10-C30-Fe70	110	0	2	0	2
H10-C37-O1-Fe80	128	0	11	0	11
H10-C38-O1-Fe80	129	0	28	0	28
H10-C38-O2-Fe80	130	0	5	0	5
H11-Fe5	16	0	1	87	88
H11-Fe16	27	0	0	1	1
H11-Fe21	32	0	0	14	14
H11-O1-Fe4	16	0	0	2	2
H11-O1-Fe20	32	0	0	1	1
H11-C38-O1-Fe80	130	0	3	0	3
H12-Fe19	31	0	0	40	40
H12-Fe32	44	0	26	1	27
H12-O2-Fe17	31	0	0	1	1
H12-C1-Fe31	44	0	105	1	106
H12-C1-O1-Fe30	44	0	1	0	1
H12-C1-O2-Fe29	44	0	3	0	3
H12-C3-O6	21	0	20	63	83
H12-C4-O1	17	1	0	0	1
H12-C4-O2	18	7	0	0	7
H12-C4-O2-Fe19	37	0	1	0	1
H12-C5-Fe20	37	0	18	2	20
H12-C6-O3	21	0	0	1	1
H12-C6-O6	24	5231	70	56	5357
H12-C7	19	8	0	0	8
H12-C7-O1	20	27	0	0	27
H12-C7-O2	21	46	0	0	46
H12-C7-O3	22	0	1	1	2
H12-C8	20	10	0	0	10
H12-C8-O1	21	28	0	0	28
H12-C8-O2-Fe15	37	0	1	0	1
H12-C8-O3	23	0	3	1	4

H12-C9	21	45	0	0	45
H12-C9-O1	22	0	7	2	9
H12-C10	22	0	4	1	5
H12-C10-Fe15	37	0	18	0	18
H12-C10-O1-Fe14	37	0	3	0	3
H12-C12-O4	28	0	0	2	2
H12-C12-O6	30	0	2	0	2
H12-C13-O5	30	0	5	6	11
H12-C14-O4	30	0	16	5	21
H12-C15-Fe35	62	0	55	0	55
H12-C15-O3	30	0	7	1	8
H12-C24-Fe39	75	0	22	0	22
H13-Fe16	29	0	167	221	388
H13-Fe19	32	0	0	5	5
H13-O1-Fe15	29	0	5	5	10
H13-O2-Fe14	29	0	1	7	8
H13-C2-Fe16	31	0	10	0	10
H13-C2-O1-Fe15	31	0	1	0	1
H13-C5-Fe22	40	0	6	0	6
H13-C17-Fe25	55	0	46	1	47
H14-Fe16	30	0	0	10	10
H14-Fe17	31	0	0	8	8
H14-Fe18	32	0	0	8	8
H14-O2-Fe14	30	0	0	1	1
H14-O2-Fe20	36	0	0	1	1
H14-O7	21	0	1	756	757
H14-C1-Fe21	36	0	0	14	14
H14-C1-O2-Fe19	36	0	0	1	1
H14-C2-Fe20	36	0	0	36	36
H14-C2-Fe40	56	0	1	0	1
H14-C2-O2-Fe18	36	0	0	2	2
H14-C4-O4	22	0	8	0	8
H14-C7-O3	24	0	1	0	1
H14-C8	22	2	0	0	2
H14-C8-O1	23	1	0	0	1
H14-C8-O2	24	0	3	1	4
H14-C8-O3	25	0	1	0	1
H14-C9	23	54	0	0	54
H14-C10-O4	28	0	1	0	1
H14-C12-O6	32	0	4	0	4
H14-C13-O5	32	0	7	1	8
H14-C14-O4	32	0	2	2	4
H14-C15-O3	32	0	7	14	21
H14-C16-O2	32	0	5	6	11
H15-Fe6	21	0	33	0	33

H15-Fe16	31	0	0	9	9
H15-Fe17	32	0	0	19	19
H15-O1-Fe5	21	0	1	0	1
H15-O1-Fe15	31	0	0	1	1
H15-O1-Fe16	32	0	0	2	2
H15-C1-Fe16	32	0	0	5	5
H15-C1-O2-Fe20	38	0	0	1	1
H15-C2-Fe21	38	0	0	17	17
H15-C2-O2-Fe19	38	0	0	1	1
H15-C4-Fe19	38	0	0	24	24
H15-C4-O2-Fe17	38	0	0	1	1
H15-C9-O2-Fe14	40	0	1	0	1
H15-C11-Fe14	40	0	40	1	41
H15-C11-O2-Fe12	40	0	1	1	2
H16-Fe5	21	0	44	1	45
H16-Fe16	32	0	1	44	45
H16-O1-Fe15	32	0	0	1	1
H16-O2-Fe3	21	0	2	0	2
H16-O2-Fe14	32	0	0	5	5
H16-O8	24	0	14	3911	3925
H16-C2-Fe16	34	0	21	0	21
H16-C2-Fe20	38	0	26	0	26
H16-C2-O1-Fe15	34	0	1	0	1
H16-C2-O1-Fe19	38	0	1	0	1
H16-C4-Fe20	40	0	10	0	10
H16-C4-O2-Fe18	40	0	1	0	1
H16-C7-O1	24	1	0	0	1
H16-C8-O1	25	38	0	0	38
H16-C8-O2	26	0	5	0	5
H16-C9	25	18	0	0	18
H16-C10	26	2	0	0	2
H16-C10-O1	27	0	2	0	2
H16-C13-O5	34	0	13	1	14
H16-C14-O4	34	0	18	4	22
H16-C16-O2	34	0	2	3	5
H16-C17-O1	34	0	6	3	9
H16-C18	34	0	3	0	3
H17-Fe15	32	0	0	9	9
H17-C1-Fe26	44	0	51	0	51
H17-C1-O1-Fe25	44	0	1	0	1
H17-C1-O2-Fe24	44	0	3	0	3
H17-C2-Fe16	35	0	19	0	19
H17-C2-O1-Fe20	40	0	1	0	1
H17-C2-O2-Fe14	35	0	1	0	1
H17-C3-Fe20	40	0	15	0	15

H17-C4-Fe21	42	0	0	24	24
H17-C5-Fe24	46	0	7	0	7
H18-Fe13	31	0	0	4	4
H18-C1-Fe11	30	0	74	18	92
H18-C1-Fe21	40	0	0	30	30
H18-C1-O1-Fe10	30	0	3	1	4
H18-C1-O2-Fe9	30	0	0	1	1
H18-C2-Fe16	36	0	30	0	30
H18-C2-Fe20	40	0	19	0	19
H18-C2-Fe26	46	0	4	0	4
H18-C2-O1-Fe15	36	0	1	0	1
H18-C2-O2-Fe14	36	0	1	0	1
H18-C9	27	1	0	0	1
H18-C9-O5	32	0	1	0	1
H18-C10	28	0	3	0	3
H18-C13-O5	36	0	3	0	3
H18-C14-O4	36	0	10	2	12
H18-C15-O3	36	0	21	3	24
H18-C16-O2	36	0	4	1	5
H19-Fe12	31	0	145	3	148
H19-Fe13	32	0	0	3	3
H19-Fe21	40	0	0	19	19
H19-O1-Fe11	31	0	6	0	6
H19-O2-Fe10	31	0	4	0	4
H19-C2-Fe20	41	0	8	0	8
H19-C2-Fe21	42	0	0	16	16
H19-C2-O2-Fe19	42	0	0	1	1
H20-C2-Fe67	89	0	1	0	1
H20-C13-O5	38	0	1	0	1
H20-C14-O4	38	0	2	0	2
H20-C15-O3	38	0	4	1	5
H20-C16-O2	38	0	19	0	19
H22-C14-O4	40	0	1	2	3
H22-C17-O1	40	0	4	2	6
H22-C18	40	0	7	2	9
H23-Fe8	31	0	10	4	14
H23-Fe9	32	0	15	8	23
H23-O1-Fe7	31	0	1	0	1
H23-O1-Fe8	32	0	1	0	1
H24-Fe8	32	0	0	2	2
H24-C2-Fe20	46	0	34	0	34
H24-C2-O1-Fe19	46	0	2	0	2
H24-C2-O2-Fe18	46	0	1	0	1
H24-C12-O12	48	1	0	0	1
H24-C16-O2	42	0	5	0	5

H26-C2-Fe40	68	0	6	0	6
H27-C2-Fe35	64	0	17	0	17
H27-C2-Fe36	65	0	21	0	21
H27-C2-Fe58	87	0	0	3	3
H29-C2-Fe39	70	0	2	0	2
H30-O15	45	124	4	94	222
H33-C2-Fe40	75	0	7	0	7
H34-C6-Fe40	80	0	2	0	2
H34-C10-Fe48	92	0	1	0	1
H35-C2-Fe30	67	0	1	0	1
H37-C2-Fe30	69	0	1	0	1
H38-C2-Fe45	85	0	3	0	3
H40-C2-Fe45	87	0	2	0	2
H41-C2-Fe39	82	0	18	0	18
H42-C2-Fe40	84	0	36	0	36
H44-C2-Fe39	85	0	2	0	2
H45-C2-Fe40	87	0	33	2	35
H46-C2-Fe40	88	0	5	0	5
H47-C2-Fe40	89	0	26	0	26
H48-C2-Fe40	90	0	4	0	4
H50-C2-Fe48	100	0	4	0	4
H52-C2-Fe48	102	0	5	0	5
total	--	9564	17506	11685	38755

Benchmark of G-NN potential against DFT calculations

Table S2. Benchmark of NN calculations for FeC_x systems against DFT results. Listed data includes total atom number per cell (N_{atom}), DFT total energy (E_{DFT}), NN total energy (E_{NN}) and energy differences between DFT total energy and NN total energy (E_{diff}, meV/atom).

	N_{atom}	E_{DFT} (eV)	E_{NN} (eV)	E_{diff} (meV/atom)
Surface				
1	124	-1030.65	-1030.76	-0.95
2	328	-2702.38	-2702.30	0.23
3	116	-954.97	-954.96	0.15
4	116	-953.89	-953.84	0.40
5	200	-1656.32	-1655.92	2.01
6	136	-1118.18	-1118.09	0.66
7	136	-1116.39	-1116.27	0.86
8	140	-1144.81	-1144.67	1.01
9	113	-928.01	-927.90	0.98
TS sampling for CO dissociation				
10	126	-1044.76	-1044.66	0.76
11	125	-1036.61	-1036.56	0.38
12	125	-1036.64	-1036.63	0.11
13	117	-961.19	-961.15	0.28
14	117	-961.18	-961.16	0.11
15	118	-969.57	-969.62	-0.39
16	118	-968.36	-968.26	0.83
17	117	-960.09	-960.04	0.36
18	117	-959.94	-960.27	-2.77
19	117	-959.98	-960.10	-0.95
20	202	-1670.95	-1670.39	2.81
21	201	-1662.79	-1662.50	1.47
22	201	-1662.79	-1662.28	2.55
23	138	-1132.78	-1132.77	0.09
24	137	-1124.35	-1124.29	0.42
25	138	-1131.39	-1131.23	1.14
26	137	-1122.98	-1122.82	1.15
27	142	-1160.16	-1159.80	2.53
28	141	-1151.30	-1151.19	0.73
29	115	-943.03	-942.69	2.88
30	114	-934.13	-934.12	0.06
31	114	-934.46	-934.12	2.92
32	114	-934.57	-934.24	2.88
33	114	-934.14	-934.00	1.22
34	114	-934.14	-933.92	1.96
Overall reaction on Fe_5C_2(510)				
35	125	-1025.92	-1025.86	0.44
36	125	-1025.01	-1024.86	1.21

37	125	-1025.78	-1025.71	0.56
38	125	-1024.99	-1024.93	0.48
39	125	-1025.26	-1025.34	-0.67
40	127	-1041.76	-1041.45	2.42
41	127	-1041.70	-1041.56	1.09
42	127	-1040.57	-1040.49	0.59
43	127	-1041.90	-1041.87	0.23
44	127	-1038.43	-1038.38	0.44
45	127	-1038.32	-1038.26	0.51
46	127	-1037.95	-1037.89	0.49
47	127	-1038.68	-1038.49	1.49
48	127	-1037.97	-1037.74	1.81
49	127	-1038.18	-1038.00	1.42
50	128	-1042.22	-1041.83	3.05
51	128	-1041.78	-1041.45	2.61
52	128	-1042.36	-1042.24	0.96
53	128	-1041.79	-1041.71	0.66
54	128	-1042.03	-1042.06	-0.23
55	130	-1055.22	-1054.98	1.83
56	130	-1054.67	-1054.42	1.95
57	130	-1055.31	-1054.92	2.98
58	131	-1058.93	-1058.69	1.86
59	131	-1058.39	-1058.33	0.42
60	131	-1058.73	-1058.52	1.57
61	128	-1041.46	-1041.07	3.04
62	128	-1041.47	-1041.17	2.30
63	129	-1045.29	-1045.08	1.65
64	129	-1045.06	-1044.97	0.67
65	129	-1045.74	-1045.53	1.67
66	129	-1045.40	-1045.19	1.61
67	129	-1045.08	-1044.81	2.09
68	129	-1045.57	-1045.32	1.93
69	130	-1049.50	-1049.23	2.06
70	127	-1038.43	-1038.38	0.44
71	127	-1037.86	-1037.79	0.60
72	127	-1037.81	-1037.79	0.15
73	127	-1038.06	-1038.01	0.41
74	128	-1042.00	-1041.94	0.42
75	128	-1041.42	-1041.40	0.21
76	128	-1041.36	-1041.39	-0.28
77	128	-1041.87	-1041.92	-0.34
78	129	-1045.81	-1045.82	-0.03
79	129	-1044.91	-1044.94	-0.20
80	130	-1049.95	-1049.90	0.42
81	126	-1033.30	-1033.28	0.18

82	127	-1036.81	-1036.73	0.60
83	127	-1035.75	-1035.77	-0.15
84	127	-1036.97	-1036.89	0.67
85	127	-1037.05	-1037.02	0.17
86	127	-1035.72	-1035.53	1.52
87	127	-1036.96	-1036.89	0.60
88	128	-1040.38	-1040.40	-0.11
89	128	-1039.68	-1039.71	-0.22
90	128	-1040.84	-1040.76	0.64
91	129	-1047.63	-1047.56	0.54
92	129	-1047.52	-1047.47	0.32
93	129	-1047.52	-1047.50	0.11
94	129	-1048.02	-1047.99	0.23
95	128	-1049.42	-1049.20	1.79
96	128	-1049.12	-1048.84	2.20
97	128	-1048.24	-1048.26	-0.18
98	128	-1048.45	-1048.38	0.55
99	129	-1053.03	-1052.97	0.45
100	129	-1052.83	-1052.79	0.36
101	129	-1052.04	-1052.01	0.19
102	129	-1052.18	-1052.08	0.71
103	129	-1052.63	-1052.57	0.45
104	129	-1051.77	-1051.85	-0.66
105	129	-1052.16	-1052.09	0.53
106	129	-1052.00	-1051.94	0.45
107	129	-1051.34	-1051.33	0.08
108	129	-1052.28	-1052.21	0.54
109	128	-1042.07	-1041.98	0.67
110	128	-1041.21	-1041.12	0.66
111	129	-1046.06	-1046.00	0.46
112	129	-1044.94	-1044.99	-0.44
113	128	-1042.06	-1042.04	0.16
114	128	-1041.75	-1041.86	-0.81
115	128	-1042.13	-1042.17	-0.30
116	129	-1044.94	-1044.93	0.07
117	129	-1045.70	-1045.70	-0.05
118	130	-1049.72	-1049.65	0.55
119	130	-1049.56	-1049.56	-0.04
120	130	-1048.34	-1048.45	-0.85
121	130	-1048.90	-1048.75	1.13
122	130	-1048.36	-1048.30	0.50
123	131	-1052.75	-1052.63	0.93
124	131	-1052.48	-1052.28	1.54
125	131	-1052.16	-1052.24	-0.66
126	125	-1024.58	-1024.64	-0.46

127	127	-1037.48	-1037.50	-0.20
128	128	-1041.03	-1040.97	0.42
129	129	-1045.54	-1045.64	-0.75
130	129	-1044.61	-1044.54	0.54
131	126	-1029.71	-1029.65	0.50
132	126	-1028.84	-1028.71	1.02
133	126	-1029.02	-1028.92	0.81
134	127	-1032.87	-1032.71	1.23
135	127	-1032.04	-1031.88	1.21
136	127	-1032.60	-1032.54	0.47
137	128	-1036.56	-1036.45	0.89
138	128	-1035.70	-1035.76	-0.41
Interface				
139	52	-441.34	-441.34	0.03
140	60	-507.35	-507.34	0.21
141	68	-576.73	-576.77	-0.52
142	84	-711.32	-711.27	0.59
143	72	-609.45	-609.45	0.06
144	76	-645.41	-645.40	0.18

* Root mean square error between DFT energy and NN energy is 1.18 meV/atom.

Table S3. Comparison between the barrier (E_a) of key reactions on Fe_5C_2(510) from DFT and NN calculations.

reaction	E_a (eV)		Diff(eV)
	DFT	NN	
CH_{Cv} -> $CH+C_v$	0.78	0.77	-0.02
CO_{Cv} -> $C_{Cv}+O$	1.19	1.07	-0.12
$C_{Cv}+CH$ -> CCH_{Cv}	0.48	0.53	0.05
$CH_{Cv}+CH$ -> $CHCH_{Cv}$	0.38	0.33	-0.05
$C_{Cv}+CCH_3$ -> $CCCH_{3\ Cv}$	0.55	0.55	0.00
CH_3+H -> CH_4	0.90	0.90	0.00
$CCH_{2\ Cv}+H$ -> $CCH_{3\ Cv}$	0.44	0.45	0.01
$CCH_{2\ Cv}+H$ -> $CHCH_{2\ Cv}$	0.75	0.71	-0.04
$CHCH_2+H$->CH_2CH_2	0.66	0.69	0.03
O+H -> OH	1.06	0.90	-0.16
$O+CH_{Cv}$ -> $OH+C_{Cv}$	1.33	1.19	-0.13
OH+H -> H_2O	0.70	0.68	-0.03
CO+O -> CO_2	1.19	0.95	-0.24
COOH -> CO_2+H	1.28	1.11	-0.17
$COOH+C_{Cv}$ -> CO_2+CH_{Cv}	0.86	0.64	-0.23

1.2. Gibbs free energy correction

The Gibbs free energy G of bulks/surfaces can be approximated by their DFT total energy E(DFT) with the appropriate inclusion of zero-point-energy (ZPE) since it is known that the vibration entropy and the PV term contributions of solid phases are negligibly small. The chemical potential μ for gas phase molecules can be calculated as follows:

$$\mu(T, P) = E(DFT) + ZPE + \Delta H(0 \rightarrow 298\ K, P_0) + \Delta H(298\ K \rightarrow T, P_0) - TS(T, P_0) + k_B T \ln \frac{P}{P_0} \quad (4)$$

where enthalpy (H) and entropy (S) terms of gas phase molecules are taken from the standard thermodynamics data in NIST Chemistry WebBook and NIST-JANAF Thermochemical Tables.

1.3. Microkinetics simulation

In our microkinetics simulation, three corrections or assumptions are made as followed:

(i) The corrections for gas-phase CO (-0.17 eV), H_2O (+0.15 eV) and CO_2 (-0.13 eV) free energies are adopted according to the enthalpy changes for the gas-phase reactions: $CO(g) + 2H_2(g) \rightarrow 1/2C_2H_4(g) + H_2O(g)$ (-1.09 and -1.41 eV calculated by the data from experiments and PBE functional, respectively) and $CO(g) + 1/2H_2(g) \rightarrow 1/4C_2H_4(g) + 1/2CO_2(g)$ (-1.03 and -1.13 eV calculated by the data from experiments and PBE functional, respectively).

(ii) The linear relationship between the adsorption free energies of CO and H and the total surface coverage of the Fe site ($\sum\theta_i^*$) are established according to our DFT energetics results (See Figure S1). For example, at 523 K:

$$G_{ad}(H) = 1.3881 \times \sum\theta_i^* - 0.5079$$

$$G_{ad}(CO) = 2.6704 \times \sum\theta_i^* - 1.2319$$

Figure S1. The linear fits (dotted lines) between the differential adsorption free energies of CO and H and the total surface coverage of Fe site at different temperatures (interval by 25 K) and the gas pressure of 1 bar from the DFT energetics results (dots).

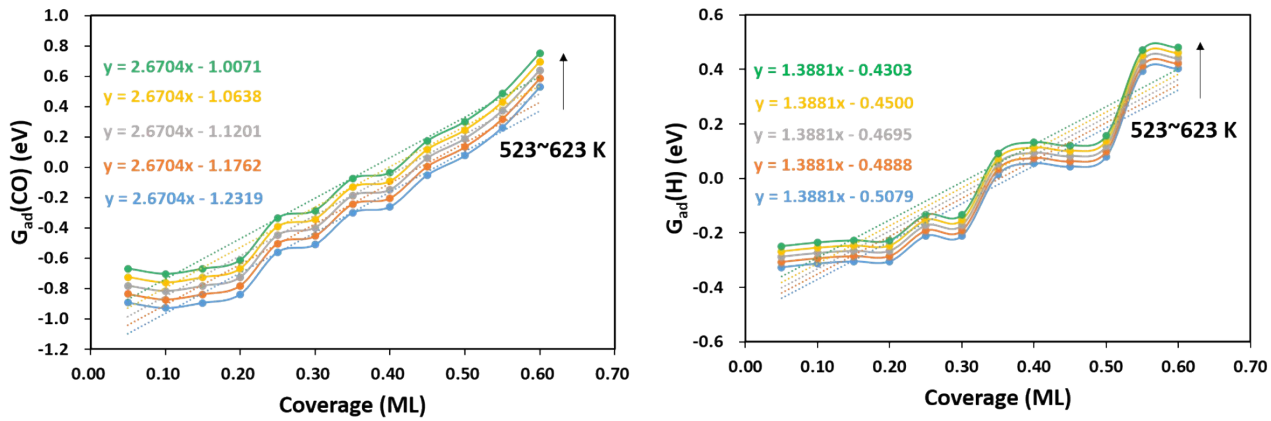

(iii) The reaction patterns and energetics for C_n-to-C_{n+1} reactions (n>2) are the same as those in C_2-to-C_3.

2. Structural details for surface model

Figure S2. Eight low energy surfaces for exploring CO dissociation channels. The A-P5 sites in six surfaces mentioned in the Discussions section are labelled.

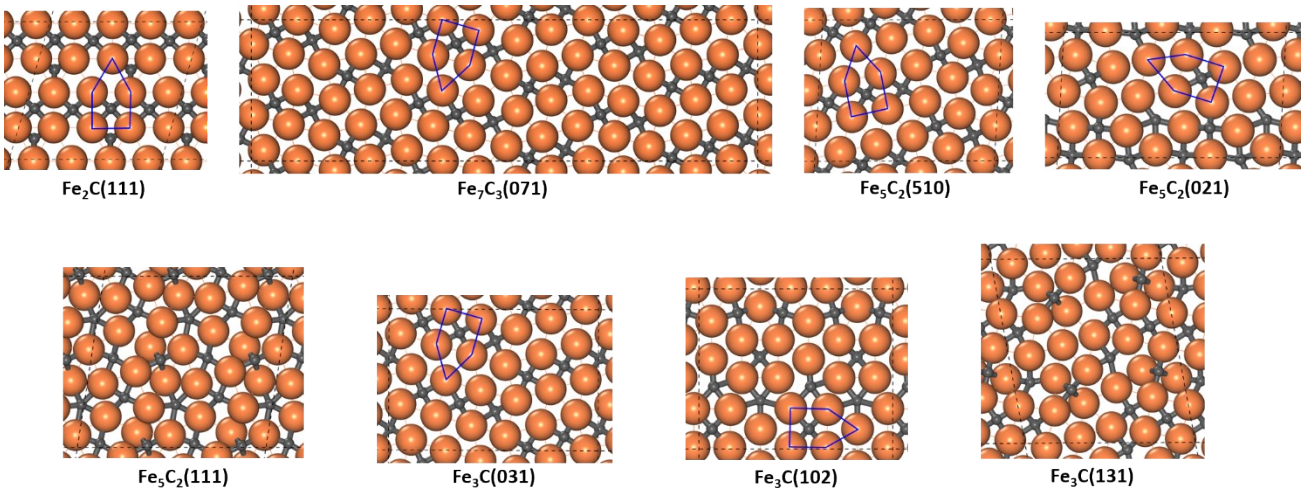

Besides A-P5 and B-P5 sites, there are other local Fe-C bonding patterns on surfaces (see Figure 2a):

(i) **Distorted five-fold site (D5).** Fe_5C_2(021), Fe_5C_2(111) and Fe_3C(131) have this site. In the D5 site, the C coordinates with a distorted Fe_4 square which shares the longest edge with an Fe_3 acute triangle. The C-Fe distance in the distorted Fe_4C square has a wide range from 1.85 to 2.22 Å.

(ii) **Pentagon (PG).** Fe_5C_2(021), Fe_5C_2(111) and Fe_3C(102) have this site. The C coordinates with five Fe atoms in a quasi-planar pentagon with five obtuse internal angles. The longest C-Fe distance in the Fe_5C pentagon is about 2.2~2.5 Å.

(iii) **Folded rectangle (FR).** Fe_5C_2(111) and Fe_3C(131) have this site. In this site, C coordinates with four Fe atoms in a folded rectangular geometry. The C-Fe distance is short (1.83~1.97 Å), but there are at least two C-Fe pairs with bond lengths up to 1.93 Å in a folded rectangle.

(iv) **Isolated square (IS).** Fe_3C(131) has this site where C coordinates with an Fe_4 square isolated by steep steps and other C sites.

3. ML-TS of CO activation on $Fe_5C_2(510)$

Figure S3. Typical TS-like structures on $Fe_5C_2(510)$ with a C vacancy sampled by ML-TS. The reaction barrier is calculated by NN potential.

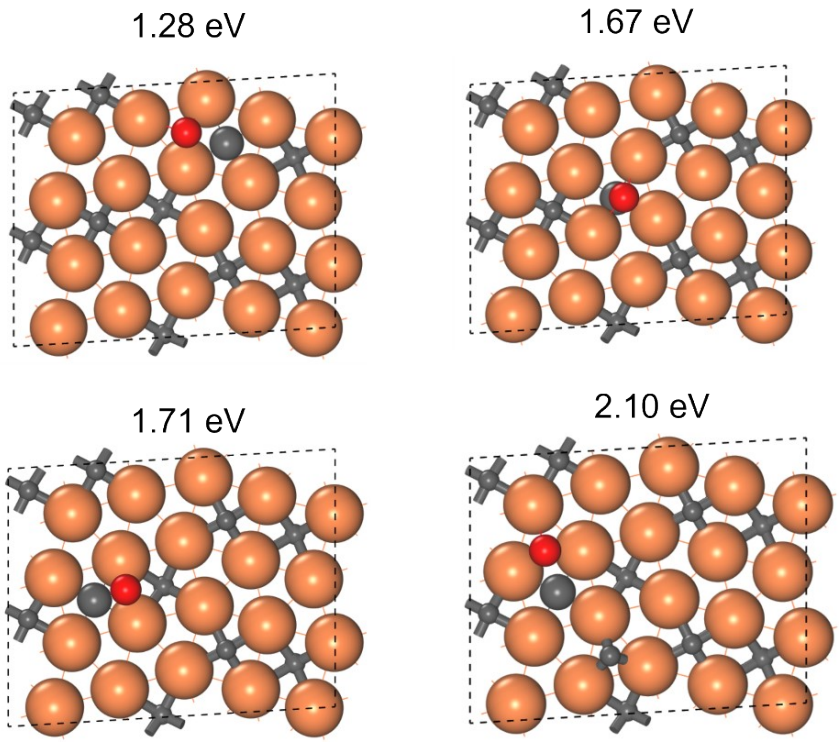

ML-TS takes into account the degrees of freedom from both molecular configurations and the surface structure reconstruction. The O atom in CO molecule absorbs on the Fe_3 (top left) or Fe_2 (bottom left) sites or links to the sinking C atom (top right) in TS. The surface reconstruction, for example, a single C atom at Fe_3 formed by C diffusion from the subsurface, or a C vacancy formed by C diffusion to the subsurface, can also be captured by ML-TS.

Figure S4. The lowest-energy TS for the terrace (left) and step (right) of Fe_5C_2(510) without a C vacancy.

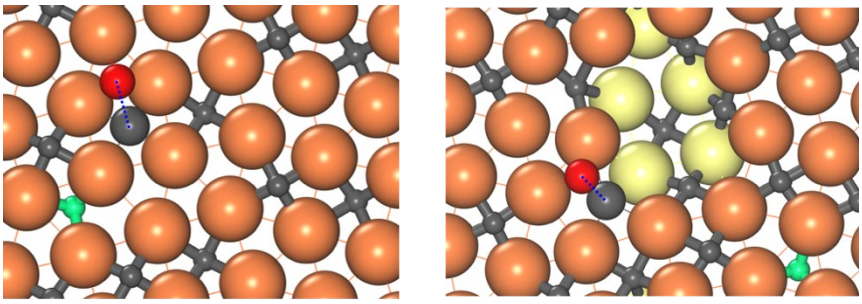

Terrace Step

CO dissociates at the surface C vacant site. The surface reconstruction occurs where a surface C atom re-locates to the subsurface site, as indicated by the green (compare with the green atom in Figure S5). The Fe atoms in the second layer is colored by yellow.

Figure S5. The ISs of CO dissociation for the terrace and step of Fe_5C_2(510) with and without a C vacancy.

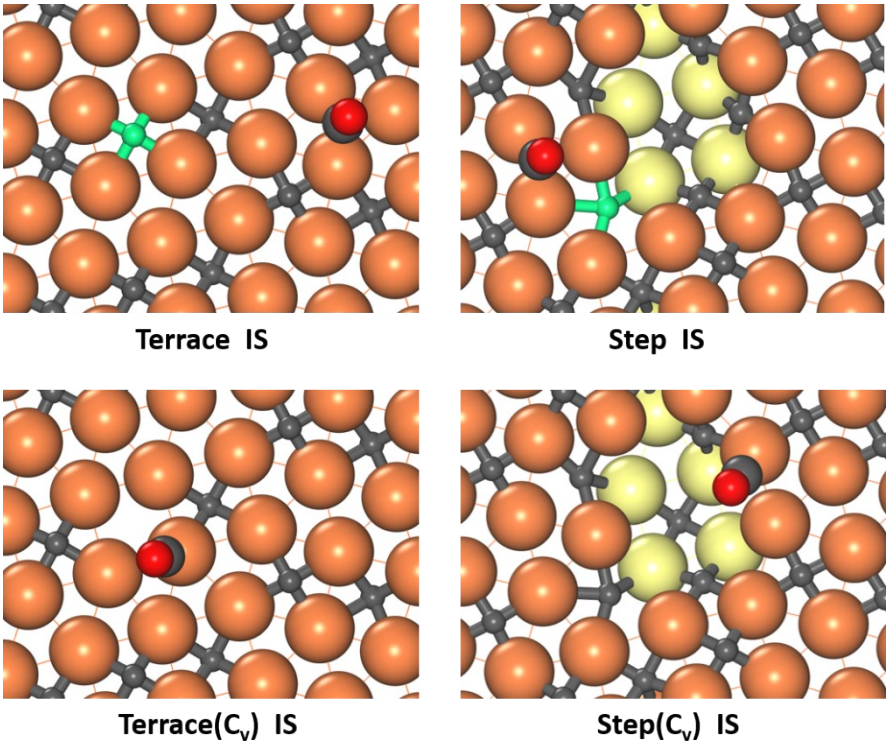

Terrace IS Step IS

Terrace(C_v) IS Step(C_v) IS

Figure S6. The IS and the TS for the lowest-energy pathway of H-assisted CO dissociation on Fe_5C_2(510) at a C vacancy site.

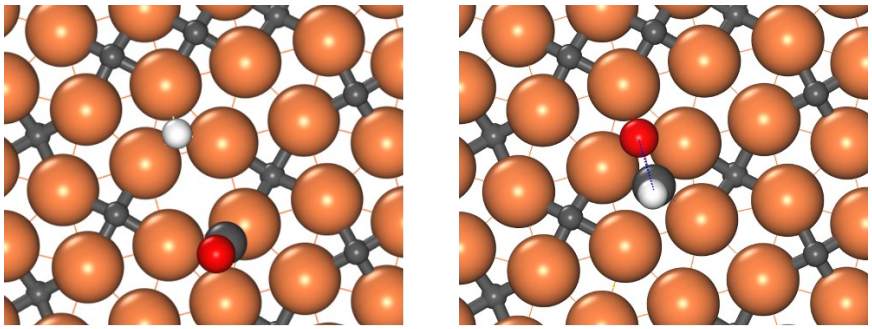

CO dissociates via the CHO intermediate in the C vacancy, which has a barrier of 1.50 eV (0.32 eV higher than C-vacancy mediated CO direct dissociation). The C-O distance is 1.66 Å in TS.

4. Reaction pathways for C-C coupling, O removal and C_2H_4 formation

Figure S7. TSs for C-C couplings on Fe_5C_2(510). The C-C distance is denoted by blue line.

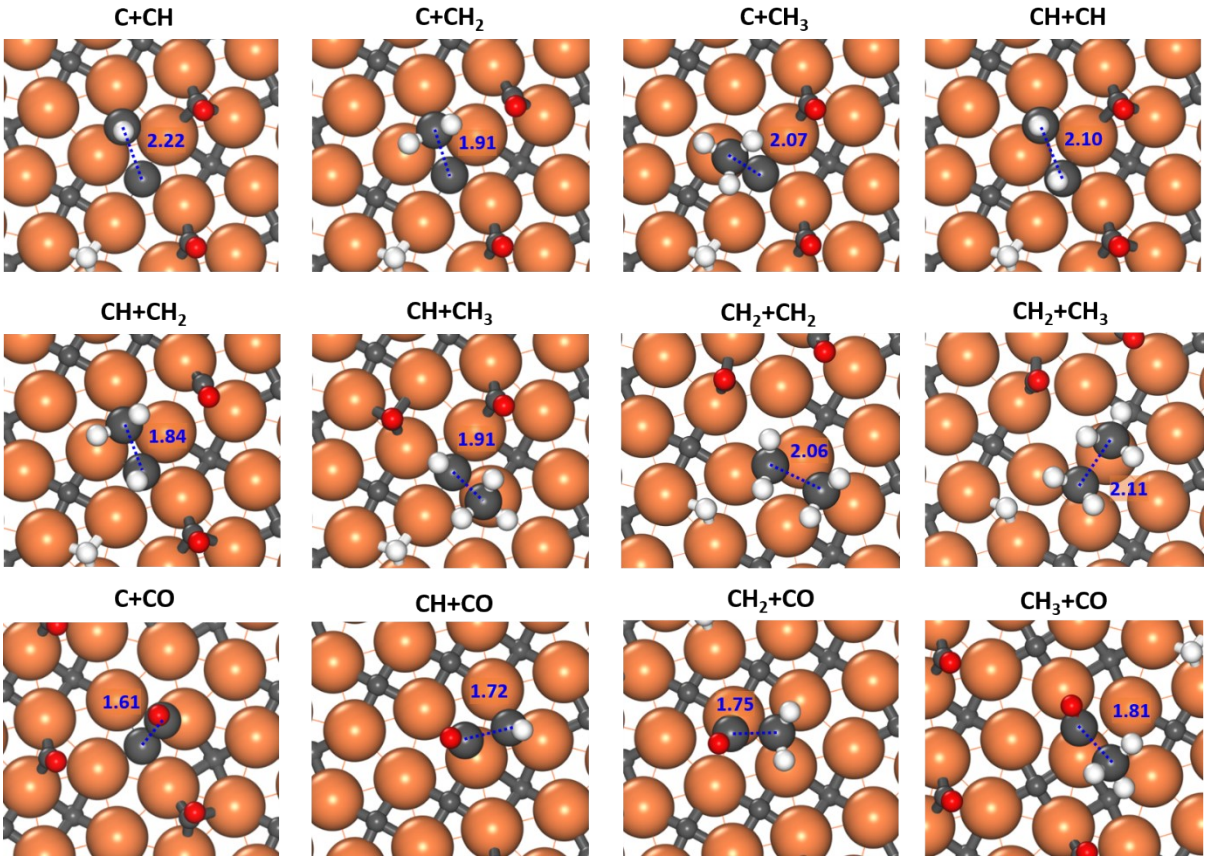

Table S4. The reaction free energy barrier (G_a) and reaction free energy (ΔG) of 9 key reactions at different coverages.

Reaction	0.05 ML CO + 0.05 ML H		0.20 ML CO + 0.05 ML H		0.25 ML H	
	G_a (eV)	ΔG (eV)	G_a (eV)	ΔG (eV)	G_a (eV)	ΔG (eV)
CO_{Cv} -> C_{Cv}+O	0.99	-0.66	1.16	-0.13	1.26	-0.31
C_{Cv}+CH -> CCH_{Cv}	0.70	0.02	0.48	-0.23	0.64	-0.03
CH_{Cv}+CH -> $CHCH_{Cv}$	0.52	0.22	0.37	-0.01	0.53	0.13
$CHCH_{2\ Cv}$ -> $CHCH_2$+C_v	0.56	-0.21	0.20	-0.44	0.18	-0.28
$CHCH_2$+H -> CH_2CH_2	0.83	0.02	0.66	0.04	0.68	0.18
C_{Cv}+CCH_3 -> $CCCH_{3\ Cv}$	0.79	0.61	0.54	-0.07	0.69	0.10
CH+H -> CH_2	0.74	0.23	0.58	0.17	0.62	0.20
CH_2+H -> CH_3	0.78	-0.08	0.62	-0.04	0.71	-0.06
CH_3+H -> CH_4	0.98		0.90		0.99	

Figure S8. Free energy profile for O removal on Fe_5C_2(510). The reaction conditions are set at T = 523 K, P = 2.5 MPa and H_2/CO = 2 for computing the free energies.

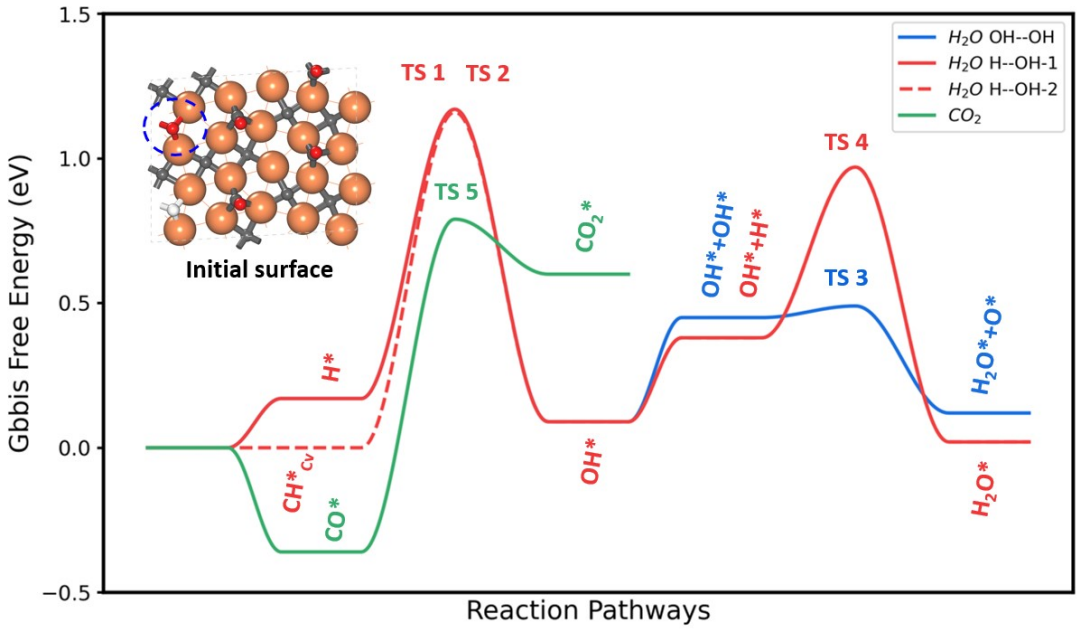

Figure S9. Free energy profile for the formation of CO_2 via COOH (CO+OH->COOH, COOH->COO+H and COOH+C->COO+C) on Fe_5C_2(510).

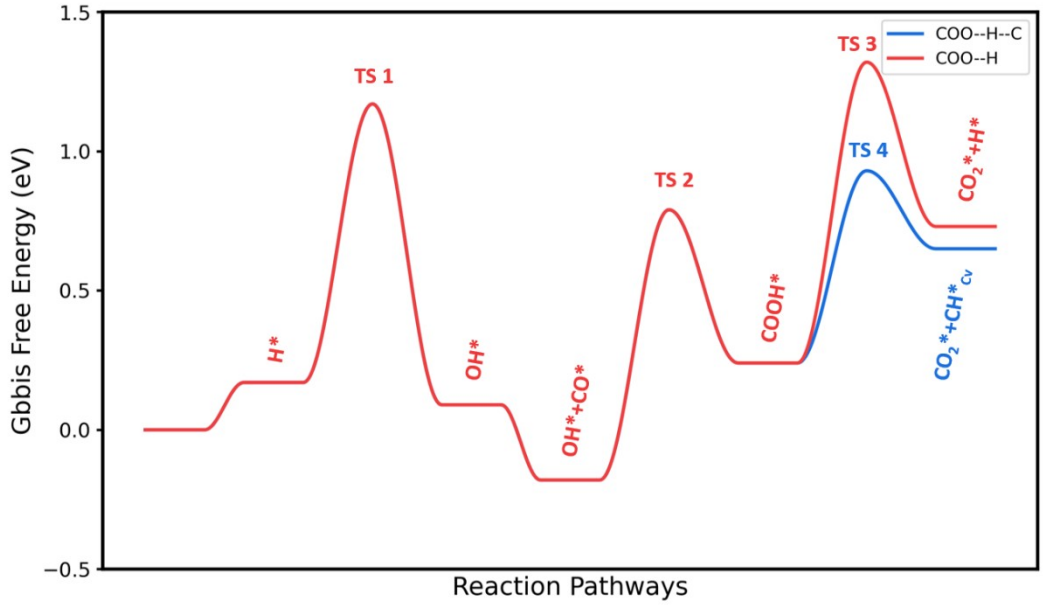

The O-removal reactions have been explored on Fe_5C_2(510) surface at different surface coverages. At relatively high surface coverages, these reactions become kinetically favorable. As shown in the inset of Figure S8, the surface coverage is 0.20 ML CO+0.05 ML H+0.05 ML O and the effective barriers for the CO_2 formation and H_2O formation are 1.11 and 1.16 eV respectively. The reactions are elaborated as follows (also see above figures).

For the elementary step of O+H, a coming H has to adsorb on a less stable 3-fold hollow site

with an endothermic of 0.17 eV (H*) and then diffuses across the top site of an Fe atom to form the new bond with O (TS1 and OH* in Figure S8, the barrier is 1.01 eV). The hydrogenation of O can also be achieved by the shift of H from C to adjacent O with a barrier of 1.16 eV (red dash line in Figure S8), in which the C-H distance increases from 1.10 Å to 1.41 Å and O-H distance decreases to 1.39 Å. Next, OH can undergo further hydrogenation (red line) or disproportionation with another OH (blue line). The former needs one more H diffusing next to the OH on the bridge site, which is endothermic by 0.29 eV (OH*+H* in Figure S8). Then, the distance between O and H shortens to 1.49 Å and finally H_2O is formed, which has a barrier of 0.59 eV. The latter occurs when two OH species meet each other with the endothermicity of 0.36 eV (OH*+OH* in Figure S8), and H shifts from one OH to the other with a barrier of 0.04 eV (TS4 in Figure S8).

For the oxidation of CO, a coming CO adsorbs on the Fe top site with an exothermicity of 0.36 eV and diffuses near to the O atom. Next, CO tilts to the O atom in the 3-fold hollow site and the distance of C and the isolated O decreases from 2.68 Å to 1.62 Å. With the shortening distance of C-O, CO_2 forms finally, which overcomes a barrier of 1.14 eV. We also considered the other reaction pathways for the formation of CO_2 via COOH (See Figure S9). Our results show that COOH->COO+H has a higher overall barrier (1.50 eV), while COOH+C->COO+C has a lower barrier of 1.11 eV.

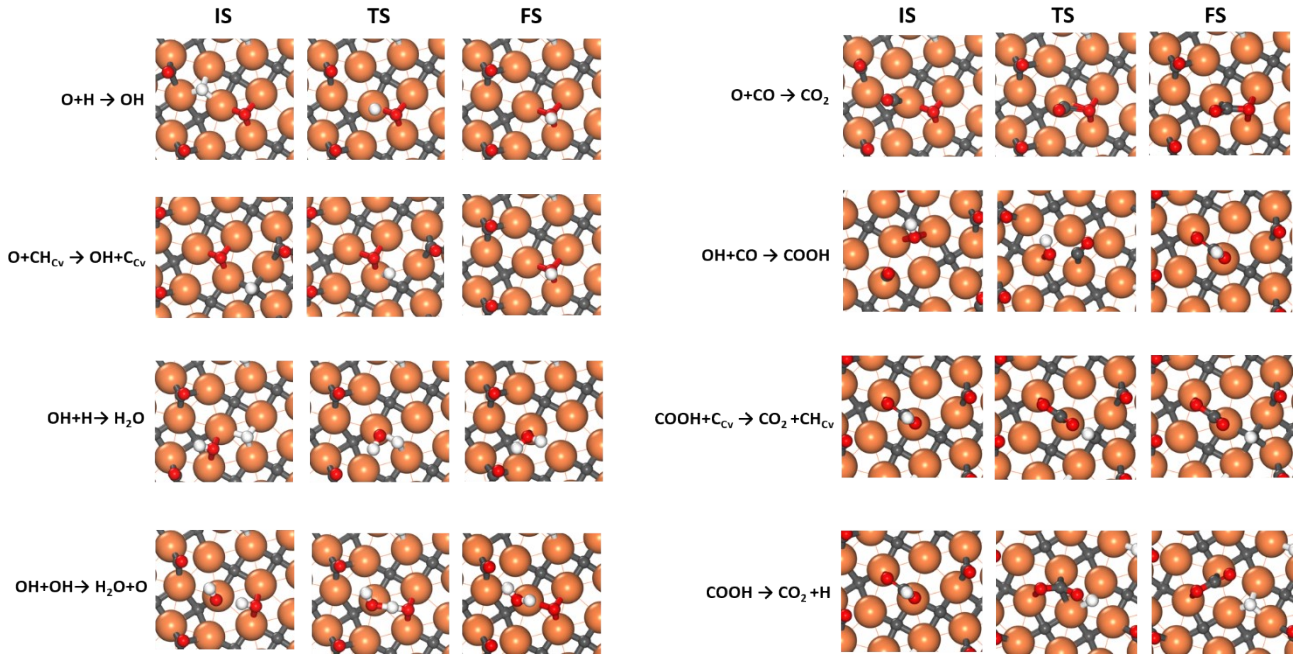

Figure S10. Structure snapshots for O removal.

Figure S11. Free energy profile for C_2H_4 formation on Fe_5C_2(510). The reaction conditions are set at T = 523 K, P = 2.5 MPa and H_2/CO = 2 for computing the free energies. The red solid and dashed lines

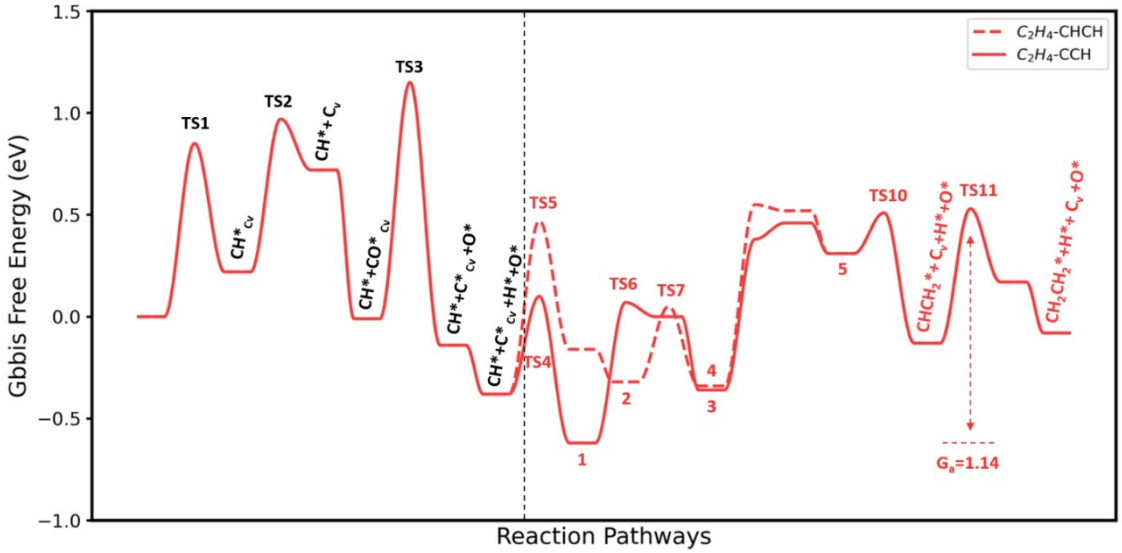

are the pathways for C_2H_4 formation via C+CH and CH+CH, respectively.

Figure S12. Structure snapshots for the reactions in Figure 4b and Figure S11.

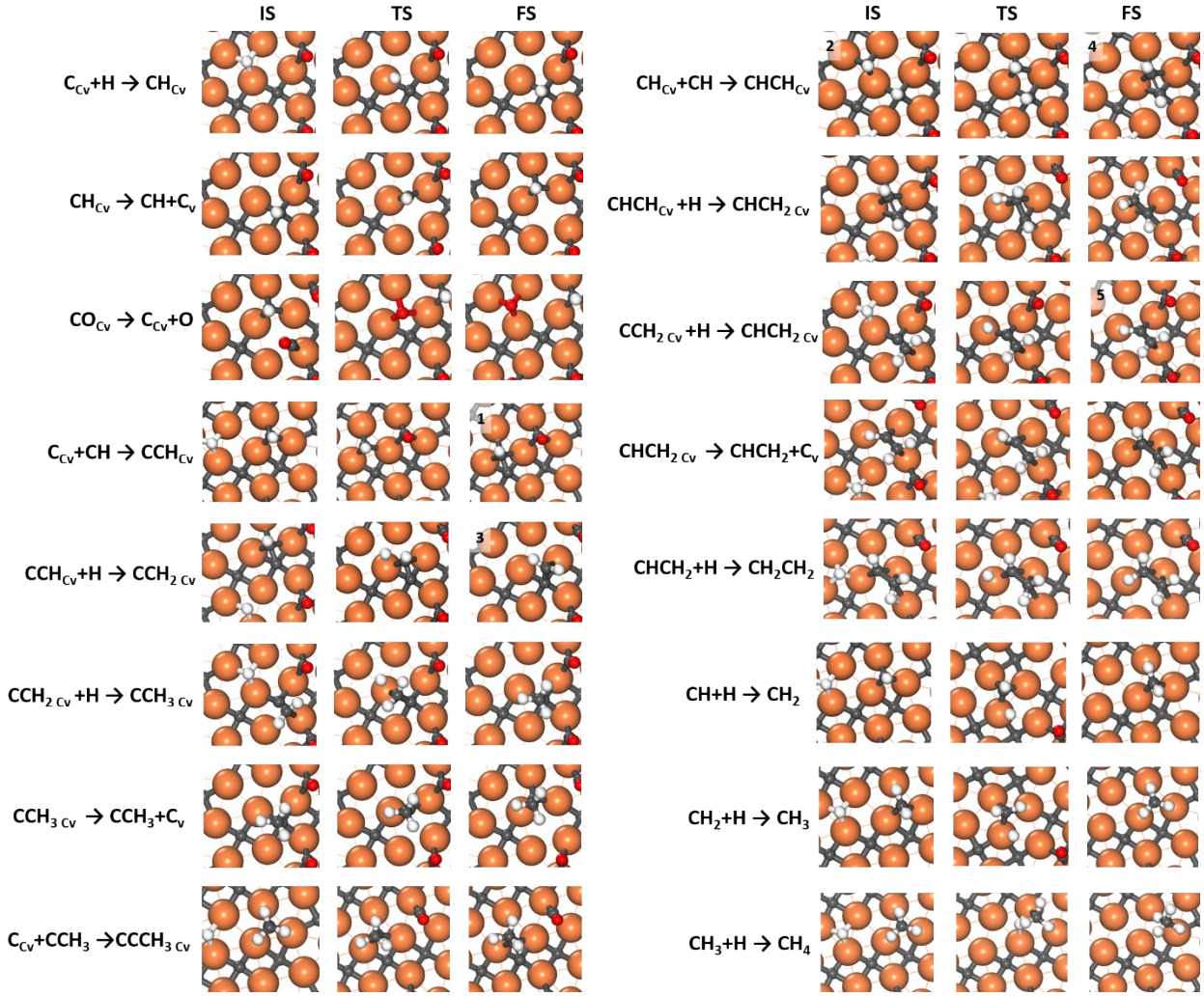

5. Microkinetics

5.1. Estimation of iron time yield (FTY)

Our calculated CO consumption rate is 1.49 s^{-1} at 548 K and 2.5 MPa syngas (H_2/CO=2). The FTY (moles of CO converted to hydrocarbons per gram of Fe per second) is commonly used in the Fe-based FT experiments to evaluate the catalytic activity. In order to compare our microkinetics results with available experimental data, our theoretical FTY is estimated as follows:

Assumption 1: The catalyst consists of the single-phase Fe_5C_2 and there are no other Fe-containing phases.

Assumption 2: the Fe_5C_2 nanoparticle is a sphere with a diameter of 20 nm.

Assumption 3: The percentage of the exposed area of Fe_5C_2(510) is 21.84% according to the Wulff construction of Fe_5C_2 nanoparticle (Figure S13).

Volume of the catalyst: $V = \left(\frac{4}{3}\right)\pi r^3 = 4.187 \times 10^{-24}\ m^3$

Surface area of the catalyst: $S = 4\pi r^2 = 1.256 \times 10^{-15}\ m^2$

Mass of the catalyst: $m = V \cdot \rho = 3.275 \times 10^{-17}\ g$

Mass of the Fe in the catalyst: $m_{Fe} = 3.015 \times 10^{-17}\ g$

Specific surface area of the catalyst (per gram Fe): $A = \frac{S}{m_{Fe}} = 41.655\ m^2 \cdot g_{Fe}^{-1}$

Specific surface area of the exposed Fe_5C_2(510): $A_{510} = 41.655 \times 21.84\% = 9.097\ m^2 \cdot g_{Fe}^{-1}$

The total number of the active site per gram Fe on Fe_5C_2(510): $N_{Fe} = 1.440 \times 10^{20}\ g_{Fe}^{-1}$

According to our microkinetics results, the rate of the consumption of CO for the hydrocarbon formation is $r_{CO\ to\ hydrocarbons} = r_{CO} - r_{CO\ to\ CO_2} = 1.495 - 0.084 = 1.411\ s^{-1}$

$$FTY = \frac{1.440 \times 10^{20} \times 1.411}{6.02 \times 10^{23}} = 3.4 \times 10^{-4}\ mol_{CO} \cdot g_{Fe}^{-1} \cdot s^{-1}$$

We also note that According to experimental literatures[8-10], the FTY of single-phase Fe_5C_2 catalyst is ~10 times larger than those of the traditional composite catalysts prepared from iron oxide, which might be due to the less concentration of the active sites in composite catalysts compared to the pure-phase Fe_5C_2 catalyst with the same content of Fe. To compare the theoretical FTY with the experimental data in Figure 5e, we assume that 10% of Fe are active:

$FTY' = FTY \times 10\%$

Figure S13. The Wulff construction of Fe_5C_2 nanoparticle.

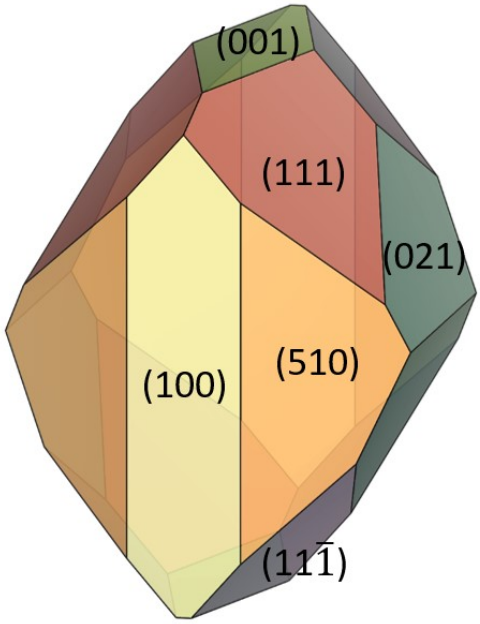

(111)	25.78%
(510)	21.84%
(021)	19.04%
(11$\bar{1}$)	12.25%
(100)	15.05%
(001)	6.04%
(010)	0%
(110)	0%

The surface free energies utilized to construct the Wulff shape are from our previous works[11, 12], which are 1.68, 1.75, 1.80, 1.81, 2.03, 2.11, 2.37 and 2.41 J/m^2 for (100), (510), (021), (111), (010), (11$\bar{1}$), (001) and (110) facets with respect to Fe_5C_2 bulk at μ_C = -6.90 eV.

5.2. Analysis of chain growth probability factor (α)

$$\alpha = \frac{r_p}{r_p + r_t} = 0.44$$

Take C_3 propagation as an example:

	r_{net}
$CCH_3\$ + * \rightarrow CCH_3* + \$$	0.031
$CCH_3* + C\$ \rightarrow CCCH_3\$ + *$	0.031
$CCCH_3\$ + H* \rightarrow CCHCH_3\$ + *$	0.031
$CCHCH_3\$ + 2H* \rightarrow C_3H_6* + \$ + *$	**0.017 (r_t)**
$CCHCH_3\$ + H* \rightarrow CCH_2CH_3\$ + *$	**0.014 (r_p)**

Table S5. The DFT reaction energy and barrier, ZPE corrections and Gibbs free energy barriers (forward and reverse) for all elementary steps (523 K) at Fe_5C_2(510). * and $ denote the Fe site and the C vacant site, respectively.

	Reaction	ΔE(FS-IS) (eV)	ΔE(TS-IS) (eV)	ΔZPE(FS-IS) (eV)	ΔZPE(TS-IS) (eV)	$G_{a,+}$ (eV)	$G_{a,-}$ (eV)
1	H_2+2* → 2H*			See Figure S1			
2	CO+* → CO*						
3	H_2+2$ → 2H$	-0.10	0.20	0.00	0.00	0.20	0.30
4	CO+$ → CO$	-0.33	0.20	0.00	0.00	0.20	0.53
5	C$+H* → CH$+*	0.14	0.91	0.08	-0.06	0.85	0.63
6	CH$+* → CH*+$	0.52	0.78	-0.02	-0.03	0.76	0.26
7	CH*+C$ → CCH$+*	-0.25	0.48	0.01	0.00	0.48	0.71
8	CCH$+H* → CCH_2+*	0.11	0.71	0.15	-0.03	0.69	0.43
9	$CCH_2$$+H* → CCH_3+*	-0.14	0.44	0.11	-0.02	0.42	0.45
10	$CCH_2$$+H* → $CHCH_2$+*	0.57	0.75	0.10	0.06	0.81	0.14
11	$CHCH_2$$+* → $CHCH_2$*+$	-0.45	0.23	0.01	-0.03	0.20	0.64
12	$CHCH_2$*+H* → CH_2CH_2*+*	-0.12	0.66	0.16	-0.01	0.66	0.61
13	CH*+CH$ → CHCH$+*	-0.01	0.38	0.00	-0.01	0.37	0.39
14	CHCH$+H* → $CHCH_2$+*	0.66	0.89	0.09	0.00	0.89	0.13
15	CH_2CH_2* → CH_2CH_2+*	-0.33	0.30	-0.05	0.00	0.30	0.69
16	CH*+H* → CH_2*+*	0.08	0.63	0.09	-0.05	0.58	0.41
17	CH_2*+H* → CH_3*+*	-0.18	0.64	0.14	-0.02	0.62	0.66
18	CH_3*+H* → CH_4+2*	-1.08	0.90	0.11	0.00	0.90	1.88
19	CO$+* → C$+O*	-0.14	1.19	0.01	-0.04	1.16	1.29
20	O*+H* → OH*+*	-0.03	1.19	0.12	-0.02	1.18	1.08
21	O*+CH$ → OH*+C$	0.07	1.33	0.00	-0.17	1.16	1.09
22	OH*+H* → H_2O*+*	-0.23	0.93	0.16	-0.05	0.88	0.95
23	2OH* → H_2O*+O*	-0.02	0.48	0.05	-0.08	0.40	0.37
24	H_2O* → H_2O+*	-0.09	0.10	-0.10	0.00	0.10	0.29
25	O*+CO* → CO_2*+*	0.98	1.19	-0.01	-0.04	1.14	0.18
26	CO*+OH* → COOH*+*	0.40	0.99	0.03	-0.02	0.97	0.55
27	COOH*+C$ → CO_2*+CH$	0.47	0.86	-0.06	-0.18	0.68	0.27
28	COOH*+* → CO_2*+H*	0.63	1.28	-0.14	-0.21	1.07	0.58
29	CO_2* → CO_2+*	-1.65	0.10	0.01	0.00	0.10	1.74
30	$CCH_3$$+* → CCH_3*+$	0.33	0.57	-0.02	-0.03	0.54	0.23
31	CCH_3*+C$ → $CCCH_3$$+*	-0.09	0.55	0.01	0.00	0.54	0.62
32	$CCCH_3$$+H* → $CCHCH_3$$+*	0.11	0.71	0.15	-0.03	0.69	0.43
33	$CCHCH_3$$+2H* → C_3H_6*+*+$	0.00	0.78	0.27	0.10	0.88	0.61
34	C_3H_6* → C_3H_6+*	-0.38	0.25	-0.05	0.00	0.25	0.69
35	$CCHCH_3$$+H* → $CCH_2CH_3$$+*	-0.14	0.44	0.11	-0.02	0.42	0.45
			…				
	C_4H_8* → C_4H_8+*	-0.43	0.20	-0.05	0.00	0.20	0.69
			…				
	C_5H_{10}* → C_5H_{10}+*	-0.48	0.15	-0.05	0.00	0.15	0.69
			…				

	C_6H_{12}* → C_6H_{12}+*	-0.53	0.10	-0.05	0.00	0.10	0.69
			…				
	C_7H_{14}* → C_7H_{14}+*	-0.58	0.05	-0.05	0.00	0.05	0.69
			…				
60	$C(CH_2)_5CH_3$\$+* → $C(CH_2)_5CH_3$*+\$	0.33	0.57	-0.02	-0.03	0.54	0.23
61	$C(CH_2)_5CH_3$*+C\$ → $CC(CH_2)_5CH_3$\$+*	-0.09	0.55	0.01	0.00	0.54	0.62
62	$CC(CH_2)_5CH_3$\$+H* → $CCH(CH_2)_5CH_3$\$+*	0.11	0.71	0.15	-0.03	0.69	0.43
63	$CCH(CH_2)_5CH_3$\$+2H* → C_8H_{16}*+*+\$	0.00	0.78	0.27	0.10	0.88	0.61
64	C_8H_{16}* → C_8H_{16}+*	-0.58	0.05	-0.05	0.00	0.05	0.69

Table S6. Surface coverage of species in microkinetics simulation on Fe_5C_2(510) at 523 K. The pressures are set at 0.83, 1.67 and 0.1 MPa for CO, H_2 and each product (including hydrocarbons, CO_2 and H_2O), respectively.

Species	Coverage (ML)
\$	8.24E-07
*	4.24E-01
C\$	1.02E-01
CO*	1.63E-01
CO\$	1.03E-02
H*	1.31E-01
H\$	1.01E-05
CH\$	2.40E-04
CH*	1.68E-03
CH_2*	1.20E-05
CH_3*	9.00E-06
CCH\$	6.64E-02
CCH_2\$	6.43E-05
CCH_3\$	3.88E-05
CCH_3*	2.05E-02
CHCH\$	1.48E-06
$CHCH_2$\$	1.64E-12
$CHCH_2$*	7.23E-04
CH_2CH_2*	7.39E-05
$CCCH_3$\$	2.92E-02
$CCHCH_3$\$	2.83E-05
CCH_2CH_3\$	1.71E-05
CCH_2CH_3*	9.03E-03
$CCCH_2CH_3$\$	1.28E-02

$CCHCH_2CH_3$\$	1.24E-05
$C(CH_2)_2CH_3$\$	7.50E-06
$C(CH_2)_2CH_3$*	3.97E-03
$CC(CH_2)_2CH_3$\$	5.64E-03
$CCH(CH_2)_2CH_3$\$	5.47E-06
$C(CH_2)_3CH_3$\$	3.30E-06
$C(CH_2)_3CH_3$*	1.75E-03
$CC(CH_2)_3CH_3$\$	2.48E-03
$CCH(CH_2)_3CH_3$\$	2.40E-06
$C(CH_2)_4CH_3$\$	1.45E-06
$C(CH_2)_4CH_3$*	7.68E-04
$CC(CH_2)_4CH_3$\$	1.09E-03
$CCH(CH_2)_4CH_3$\$	1.06E-06
$C(CH_2)_5CH_3$\$	6.38E-07
$C(CH_2)_5CH_3$*	3.38E-04
$CC(CH_2)_5CH_3$\$	4.80E-04
$CCH(CH_2)_5CH_3$\$	4.65E-07
C_3H_6*	2.44E-05
C_4H_8*	8.04E-06
C_5H_{10}*	2.65E-06
C_6H_{12}*	8.74E-07
C_7H_{14}*	2.88E-07
C_8H_{16}*	2.88E-07
O*	1.73E-03
OH*	4.58E-03
H_2O*	6.25E-03
COOH*	1.25E-07

Table S7. Degree of rate control (DRC)[13] for each elementary step.

$$DRC_i = \left(\frac{\partial ln\, r}{\partial ln\, k_i}\right)_{k_{j\neq i},\ K_i}$$

where reaction rate *r* is defined as *r(CO+H_2)*, and k_i is the rate constant for the elementary step *i*.

Reaction	DRC
H_2+2* → 2H*	7.80E-08
CO+* → CO*	-2.08E-05
CO+$ → CO$	2.06E-07
H_2+2$ → 2H$	0.00E+00
C$+H* → CH$+*	-7.99E-04
CH$+* → CH*+$	1.88E-03
CH*+C$ → CCH$+*	9.18E-06
CCH$+H* → CCH_2+*	7.00E-05
CCH_2+H* → CCH_3+*	-1.13E-06
CCH_2+H* → $CHCH_2$+*	2.13E-01
$CHCH_2$+* → $CHCH_2$*+$	2.13E-01
$CHCH_2$*+H* → CH_2CH_2*+*	1.66E-05
CH*+CH$ → CHCH$+*	-8.38E-06
CHCH$+H* → $CHCH_2$+*	-2.39E-01
CH_2CH_2* → CH_2CH_2+*	7.33E-09
CH*+H* → CH_2*+*	1.57E-06
CH_2*+H* → CH_3*+*	5.28E-04
CH_3*+H* → CH_4+2*	4.11E-02
CO$+* → C$+O*	**4.10E-01**
O*+H* → OH*+*	-5.68E-04
O*+CH$ → OH*+C$	-1.02E-04
OH*+H* → H_2O*+*	1.77E-02
2OH* → H_2O*+O*	1.20E-06
H_2O* → H_2O+*	7.06E-12
O*+CO* → CO_2*+*	4.00E-05
CO*+OH* → COOH*+*	2.59E-06
COOH*+C$ → CO_2*+CH$	2.90E-05
COOH*+* → CO_2*+H*	1.83E-08
CO_2* → CO_2+*	3.92E-05
$CCH_3$$+* → CCH_3*+$	-8.34E-06
CCH_3*+C$ → $CCCH_3$$+*	1.05E-08
$CCCH_3$$+H* → $CCHCH_3$$+*	1.56E-06
$CCHCH_3$$+2H* → C_3H_6*+*+$	5.79E-02
C_3H_6* → C_3H_6+*	6.39E-11
$CCHCH_3$$+H* → $CCH_2CH_3$$+*	-4.54E-08
$CCH_2CH_3$$+* → CCH_2CH_3*+$	-3.27E-07
CCH_2CH_3*+C$ → $CCCH_2CH_3$$+*	3.06E-08
$CCCH_2CH_3$$+H* → $CCHCH_2CH_3$$+*	1.07E-06
$CCHCH_2CH_3$$+2H* → C_4H_8*+*+$	3.36E-02
C_4H_8* → C_4H_8+*	1.20E-11

$CCHCH_2CH_3\$+H^* \rightarrow C(CH_2)_2CH_3\$+^*$	1.62E-07
$C(CH_2)_2CH_3\$+^* \rightarrow C(CH_2)_2CH_3{}^*+\$$	1.20E-06
$C(CH_2)_2CH_3{}^*+C\$ \rightarrow CC(CH_2)_2CH_3\$+^*$	2.37E-08
$CC(CH_2)_2CH_3\$+H^* \rightarrow CCH(CH_2)_2CH_3\$+^*$	6.23E-07
$CCH(CH_2)_2CH_3\$+2H^* \rightarrow C_5H_{10}{}^*+^*+\$$	1.80E-02
$C_5H_{10}{}^* \rightarrow C_5H_{10}+^*$	2.14E-12
$CCH(CH_2)_2CH_3\$+H^* \rightarrow C(CH_2)_3CH_3\$+^*$	1.32E-07
$C(CH_2)_3CH_3\$+^* \rightarrow C(CH_2)_3CH_3{}^*+\$$	9.77E-07
$C(CH_2)_3CH_3{}^*+C\$ \rightarrow CC(CH_2)_3CH_3\$+^*$	1.36E-08
$CC(CH_2)_3CH_3\$+H^* \rightarrow CCH(CH_2)_3CH_3\$+^*$	3.17E-07
$CCH(CH_2)_3CH_3\$+2H^* \rightarrow C_6H_{12}{}^*+^*+\$$	9.30E-03
$C_6H_{12}{}^* \rightarrow C_6H_{12}+^*$	3.70E-13
$CCH(CH_2)_3CH_3\$+H^* \rightarrow C(CH_2)_4CH_3\$+^*$	6.65E-08
$C(CH_2)_4CH_3\$+^* \rightarrow C(CH_2)_4CH_3{}^*+\$$	4.90E-07
$C(CH_2)_4CH_3{}^*+C\$ \rightarrow CC(CH_2)_4CH_3\$+^*$	6.16E-09
$CC(CH_2)_4CH_3\$+H^* \rightarrow CCH(CH_2)_4CH_3\$+^*$	1.36E-07
$CCH(CH_2)_4CH_3\$+2H^* \rightarrow C_7H_{14}{}^*+^*+\$$	4.69E-03
$C_7H_{14}{}^* \rightarrow C_7H_{14}+^*$	6.14E-14
$CCH(CH_2)_4CH_3\$+H^* \rightarrow C(CH_2)_5CH_3\$+^*$	1.80E-08
$C(CH_2)_5CH_3\$+^* \rightarrow C(CH_2)_5CH_3{}^*+\$$	1.33E-07
$C(CH_2)_5CH_3{}^*+C\$ \rightarrow CC(CH_2)_5CH_3\$+^*$	1.75E-09
$CC(CH_2)_5CH_3\$+H^* \rightarrow CCH(CH_2)_5CH_3\$+^*$	3.96E-08
$CCH(CH_2)_5CH_3\$+2H^* \rightarrow C_8H_{16}{}^*+^*+\$$	2.33E-03
$C_8H_{16}{}^* \rightarrow C_8H_{16}+^*$	2.98E-14

Figure S14. The steady-state rate in ln(r) as a function of temperature for H_2O and CO_2 formation.

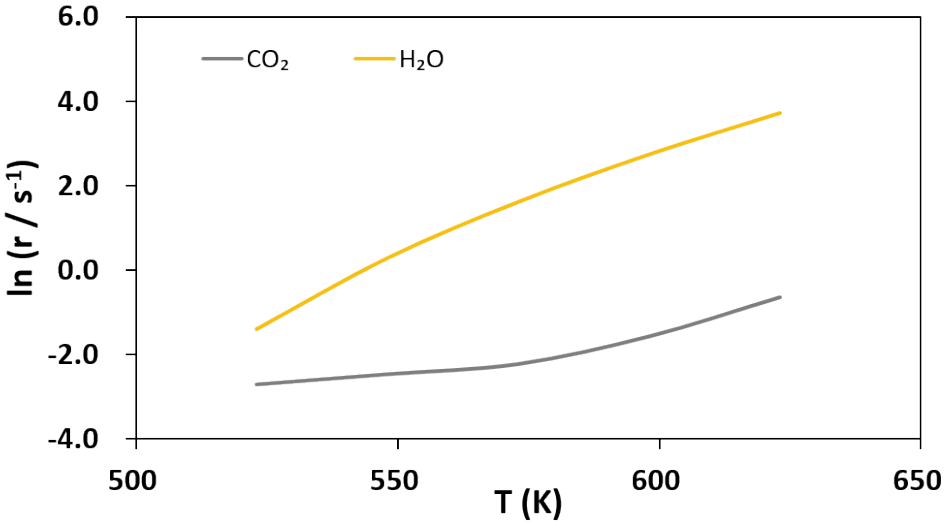

Figure S15. The apparent activation energies of C_2H_4, C_5H_{10} and C_8H_{16}.

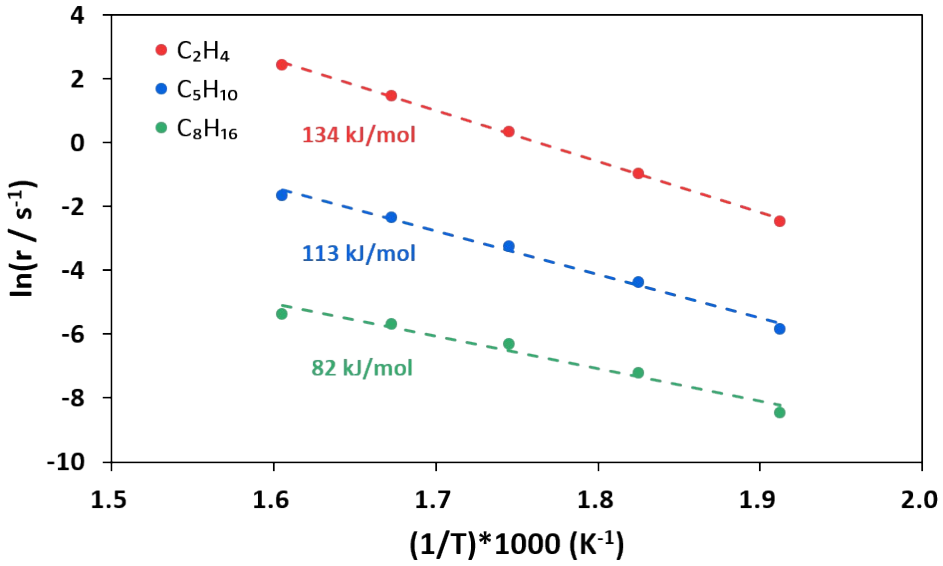

Figure S16. Influence of H_2 partial pressure on FTY at 548 K. The pressures are set at 0.25, 0.01, 0.01 and 0.1 MPa for CO, H_2O, C_8H_{16} and the other products, respectively.

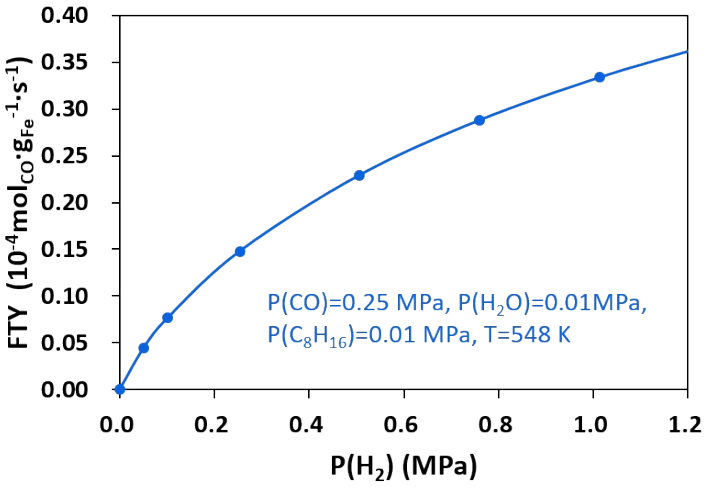

Figure S17. The reaction order of CO and H_2 calculated from the data in Figure 5e and Figure S16.

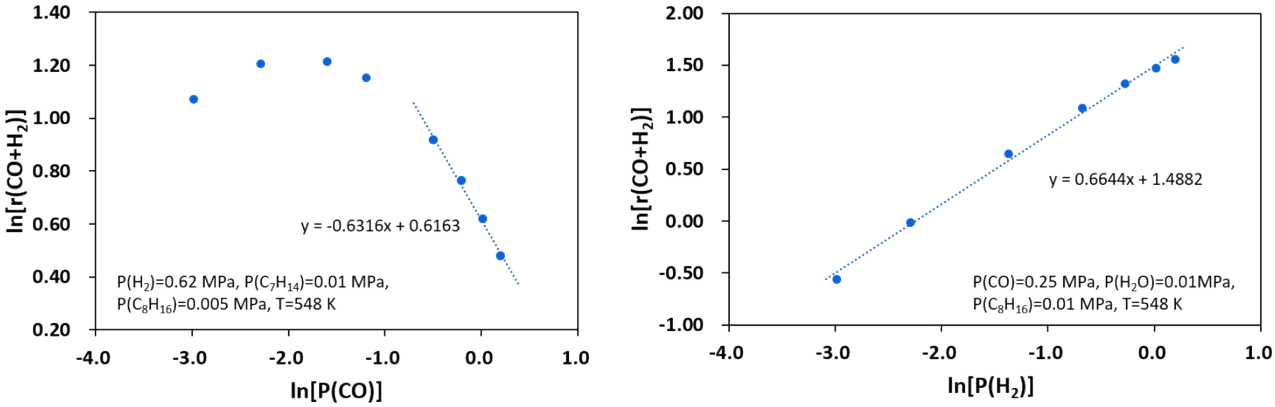

The reaction order of CO is positive at low CO pressure and then becomes negative with the increasing CO pressure. When CO partial pressure is higher than 0.6 MPa, the reaction order of CO is -0.63. The reaction order of H_2 is positive, being 0.66.

6. Properties of A-P5 sites

Table S8. TSs of C hydrogenation and CH diffusion, IS and TS of CO dissociation on the most reactive A-P5 sites in six surfaces.

Surface	TS of C hydrogenation	TS of CH diffusion	IS of CO dissociation	TS of CO dissocation
$Fe_2C(111)$	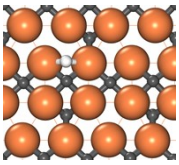	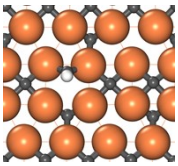	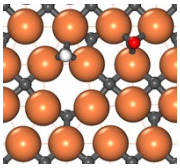	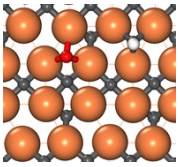
$Fe_7C_3(071)$	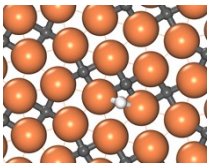	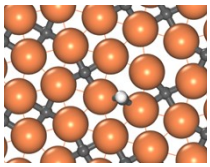	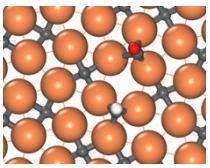	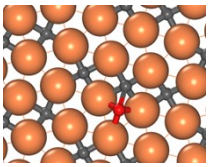
$Fe_5C_2(510)$	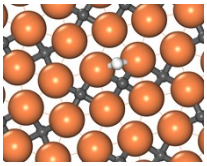	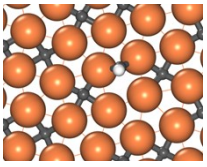	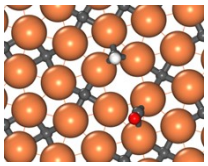	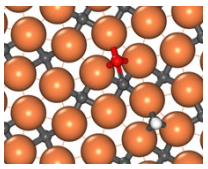
$Fe_5C_2(021)$	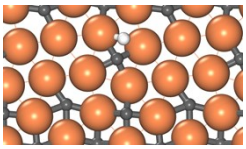	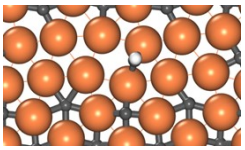	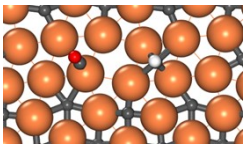	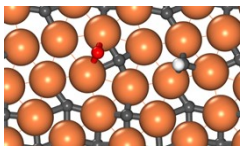
$Fe_3C(031)$	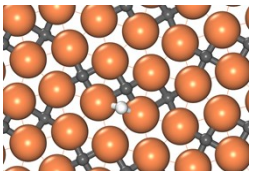	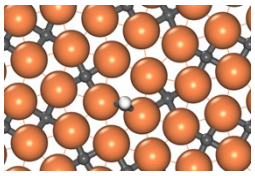	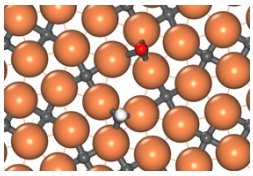	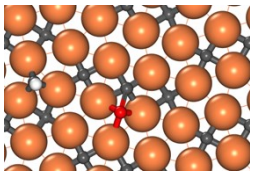
$Fe_3C(102)$	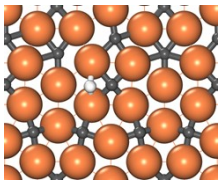	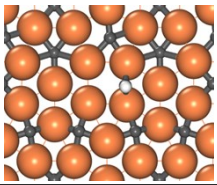	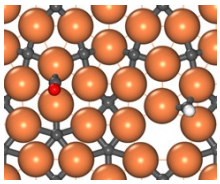	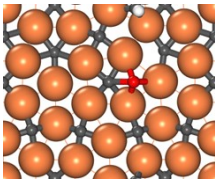

Figure S18. Relation between the reaction barrier and the descriptor of Fe-C coordination number (CN). The barriers of CH diffusion G_a(TS2) and CO dissociation G_a(TS3) are linearly related to ΔCN and CN(A-P5), respectively.

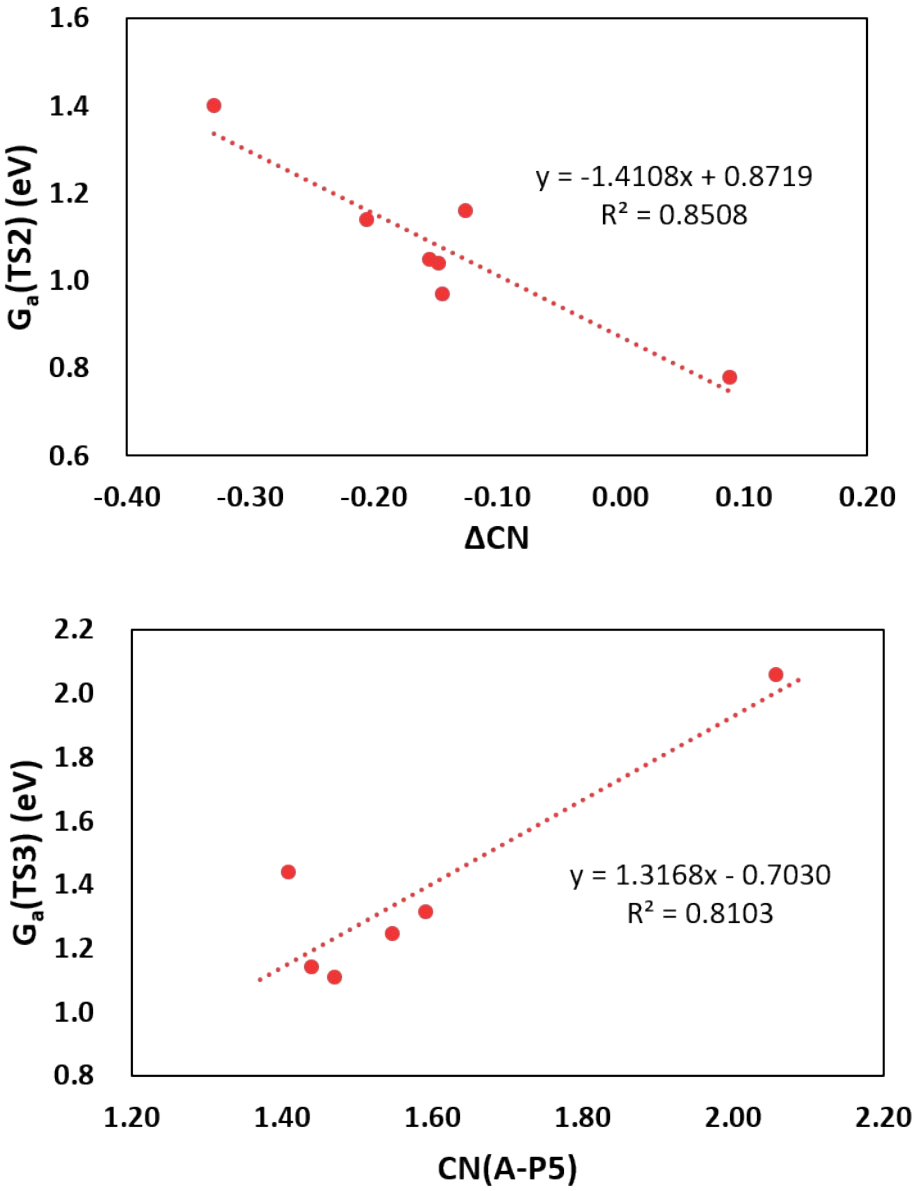

7. Interface structures

Figure S19. Other interface structures between the most stable surfaces of Fe_3C, Fe_5C_2, Fe_7C_3 and Fe_2C, i.e. $Fe_3C(010)$, $Fe_5C_2(100)$, $Fe_7C_3(010)$ and $Fe_2C(011)$.

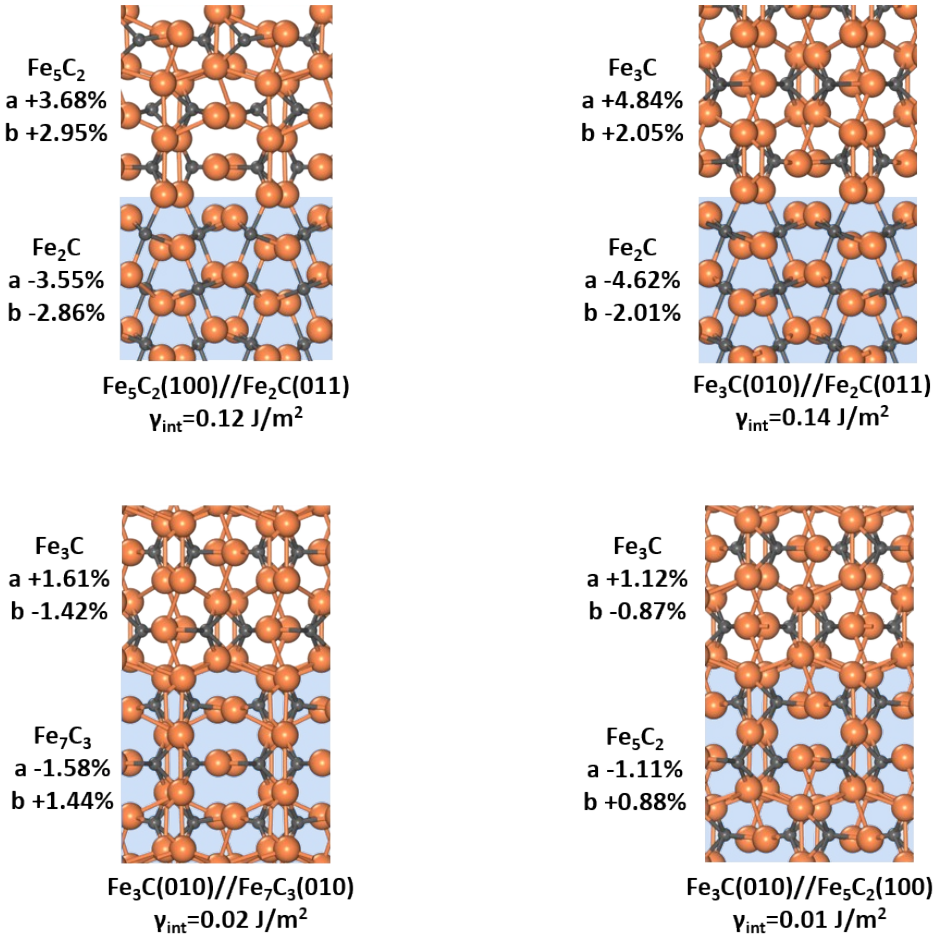

Reference:

1 S.-D. Huang, C. Shang, X.-J. Zhang and Z.-P. Liu, *Chem. Sci.* **2017**, *8*, 6327-6337.

2 S.-D. Huang, C. Shang, P.-L. Kang and Z.-P. Liu, *Chem. Sci.* **2018**, *9*, 8644-8655.

3 J. Behler and M. Parrinello, *Phys. Rev. Lett.* **2007**, *98*, 146401.

4 J. Behler, *J. Phys. Condens. Mat.* **2014**, *26*, 183001.

5 C. Shang and Z.-P. Liu, *J. Chem. Theory Comput.* **2013**, *9*, 1838-1845.

6 X.-J. Zhang, C. Shang and Z.-P. Liu, *J. Chem. Theory Comput.* **2013**, *9*, 3252-3260.

7 C. Shang, X.-J. Zhang and Z.-P. Liu, *Phys. Chem. Chem. Phys.* **2014**, *16*, 17845-17856.

8 H. Zhao, J.-X. Liu, C. Yang, S. Yao, H.-Y. Su, Z. Gao, M. Dong, J. Wang, A. I. Rykov, J. Wang, Y. Hou, W. Li and D. Ma, *CCS Chem.* **2021**, *3*, 2712–2724.

9 H. M. Torres Galvis, J. H. Bitter, C. B. Khare, M. Ruitenbeek, A. I. Dugulan and K. P. de Jong, *Science* **2012**, *335*, 835–838.

10 H. M. Torres Galvis, J. H. Bitter, T. Davidian, M. Ruitenbeek, A. I. Dugulan and K. P. de Jong, *J. Am. Chem. Soc.* **2012**, *134*, 16207–16215.

11 Q.-Y. Liu, C. Shang and Z.-P. Liu, *J. Am. Chem. Soc.* **2021**, *143*, 11109–11120.

12 Q.-Y. Liu, C. Shang and Z.-P. Liu, *J. Phys. Chem. Lett.* **2022**, *13*, 3342–3352.

13 C. T. Campbell, *ACS Catal.* **2017**, *7*, 2770–2779.